ASC Report No. 02/2007

A Posteriori Error Estimate and Adaptive Mesh-Refinement for the Cell-Centered Finite Volume Method for Elliptic Boundary Value Problems

Christoph Erath, Dirk Praetorius

Institute for Analysis and Scientific Computing
Vienna University of Technology — TU Wien
www.asc.tuwien.ac.at ISBN 978-3-902627-00-1

Most recent ASC Reports

01/2007 *Samuel Ferraz-Leite, Dirk Praetorius*
Simple A Posteriori Error Estimators for the h-Version of the Boundary Element Method

Institute for Analysis and Scientific Computing
Vienna University of Technology
Wiedner Hauptstraße 8–10
1040 Wien, Austria

E-Mail: admin@asc.tuwien.ac.at
WWW: http://www.asc.tuwien.ac.at
FAX: +43-1-58801-10196

ISBN 978-3-902627-00-1

© Alle Rechte vorbehalten. Nachdruck nur mit Genehmigung des Autors.

ASC
TU WIEN

A POSTERIORI ERROR ESTIMATE AND ADAPTIVE MESH-REFINEMENT FOR THE CELL-CENTERED FINITE VOLUME METHOD FOR ELLIPTIC BOUNDARY VALUE PROBLEMS

CHRISTOPH ERATH AND DIRK PRAETORIUS

ABSTRACT. We extend a result of NICAISE [13] for the a posteriori error estimation of the cell-centered finite volume method for the numerical solution of elliptic problems. Having computed the piecewise constant finite volume solution u_h, we compute a Morley-type interpolant $\mathcal{I}u_h$. For the exact solution u, the energy error $\|\nabla_{\mathcal{T}}(u-\mathcal{I}u_h)\|_{L^2}$ can be controlled efficiently and reliably by a residual-based a posteriori error estimator η. The local contributions of η are used to steer an adaptive mesh-refining algorithm. As model example serves the Laplace equation in 2D with mixed Dirichlet-Neumann boundary conditions.

1. Introduction

Throughout, $\Omega \subset \mathbb{R}^2$ is a bounded and connected domain with Lipschitz boundary $\Gamma := \partial\Omega$. We assume that Γ is divided into a closed Dirichlet boundary $\Gamma_D \subseteq \Gamma$ with positive surface measure and a Neumann boundary $\Gamma_N := \Gamma \backslash \Gamma_D$. We consider the elliptic model problem

$$-\Delta u = f \quad \text{in } \Omega \tag{1.1}$$

with mixed boundary conditions

$$u = u_D \quad \text{on } \Gamma_D \qquad \text{and} \qquad \partial u/\partial \mathbf{n} = g \quad \text{on } \Gamma_N. \tag{1.2}$$

Here $f \in L^2(\Omega)$, $u_D \in H^1(\Gamma_D)$, and $g \in L^2(\Gamma_N)$ are given data, and $L^2(\cdot)$ and $H^1(\cdot)$ denote the standard Lebesgue- and Sobolev-spaces equipped with the usual norms $\|\cdot\|_{L^2(\cdot)}$ and $\|\cdot\|_{H^1(\cdot)}$. The weak form of (1.1) reads: Find $u \in H^1(\Omega)$ with $u|_{\Gamma_D} = u_D$ and

$$\int_\Omega \nabla u \cdot \nabla v \, dx = \int_\Omega f v \, dx + \int_{\Gamma_N} g v \, dx \quad \text{for all } v \in H^1_D(\Omega) := \big\{ v \in H^1(\Omega) \,\big|\, v|_{\Gamma_D} = 0 \big\}. \tag{1.3}$$

Recall that there is a unique solution u which we aim to approximate by a postprocessed finite volume scheme. For technical reasons, we assume that Γ_D as well as Γ_N are connected, cf. Section 5.2 below.

Let $\mathcal{T}$ be a triangulation of Ω and $\mathcal{E}$ the set of all edges of $\mathcal{T}$. Replacing the continuous diffusion flux $\int_E \partial u/\partial \mathbf{n}_E \, ds$ by a discrete diffusion flux $F_E^D(u_h)$, the cell-centered finite volume method provides a $\mathcal{T}$-elementwise constant approximation $u_h \in \mathcal{P}^0(\mathcal{T})$ of u. The classical choice of $F_E^D(u_h)$ is based on the admissibility of the triangulation $\mathcal{T}$ in the sense of [11]. However, locally refined meshes are usually not admissible. Another choice of $F_E^D(u_h)$ is the diamond path method, which has been mathematically analyzed in [8, 9] for rectangular meshes with maximum one hanging node per edge. Optimal order of convergence $\|u -$

Date: September 6, 2007.

1991 *Mathematics Subject Classification.* 65N30, 65N15.

Key words and phrases. finite volume method, cell-centered method, diamond path, a posteriori error estimate, adaptive algorithm.

$u_h\|_{1,h} = \mathcal{O}(h)$ of the error with respect to a discrete H^1-norm $\|\cdot\|_{1,h}$ holds under the regularity assumption $u \in H^2(\Omega)$, which is usually not met in praxis.

We aim to provide a mathematical criterion for steering an adaptive mesh-refining algorithm to recover the optimal order of convergence $\mathcal{O}(N^{-1/2})$ with respect to the number $N = \#\mathcal{T}$ of elements. Following Nicaise [13], we introduce a Morley type interpolant $\mathcal{I}u_h$ which belongs to a certain $H^1(\Omega)$-nonconforming finite element space. The definition of which is a generalization of the definition in [13, Section 5] to the case of hanging nodes and mixed boundary conditions. Roughly speaking, the analytical idea is to ensure that $\mathcal{I}u_h$ has enough orthogonality properties which can be used to adapt the well-known a posteriori error analysis from the context of the finite element method, e.g., [15, 1]. For each element $T \in \mathcal{T}$ with corresponding edges $\mathcal{E}_T$, we define the refinement indicators

$$\begin{aligned}\eta_T^2 := h_T^2\|f - f_{\mathcal{T}}\|_{L^2(T)}^2 &+ \sum_{E\in\mathcal{E}_T\cap\mathcal{E}_E} h_E\|[\![\nabla_{\mathcal{T}}(\mathcal{I}u_h)]\!]\|_{L^2(E)}^2 \\ &+ \sum_{E\in\mathcal{E}_T\cap\mathcal{E}_N} h_E\Big\|\frac{\partial(u-\mathcal{I}u_h)}{\partial\mathbf{n}_E}\Big\|_{L^2(E)}^2 + \sum_{E\in\mathcal{E}_T\cap\mathcal{E}_D} h_E\Big\|\frac{\partial(u-\mathcal{I}u_h)}{\partial\mathbf{t}_E}\Big\|_{L^2(E)}^2.\end{aligned} \tag{1.4}$$

Here, $[\![\cdot]\!]$ denotes the jump, $\mathbf{n}_E$ and $\mathbf{t}_E$ denote the normal and tangential vector on E, respectively, $f_{\mathcal{T}}$ denotes the piecewise integral mean of the volume term, and h_E is the length of the edge E. We prove that the corresponding error estimator

$$\eta := \Big(\sum_{T\in\mathcal{T}} \eta_T^2\Big)^{1/2}. \tag{1.5}$$

is reliable and efficient in the sense that

$$C_{\mathrm{rel}}^{-1}\,\|\nabla_{\mathcal{T}}(u-\mathcal{I}u_h)\|_{L^2(\Omega)} \le \eta \le C_{\mathrm{eff}}\,\big[\|\nabla_{\mathcal{T}}(u-\mathcal{I}u_h)\|_{L^2(\Omega)} + \|h(f-f_{\mathcal{T}})\|_{L^2(\Omega)}\big] \tag{1.6}$$

Here, $\nabla_{\mathcal{T}}$ denotes the $\mathcal{T}$-piecewise gradient, and the constants $C_{\mathrm{eff}}, C_{\mathrm{rel}} > 0$ only depend on the shape of the elements in $\mathcal{T}$ but not on f, the local mesh-width h, or the number of elements. Moreover, the efficiency estimate holds even locally

$$\eta_T \le C_{\mathrm{eff}}\,\big[\|\nabla_{\mathcal{T}}(u-\mathcal{I}u_h)\|_{L^2(\omega_T)} + \|h(f-f_{\mathcal{T}})\|_{L^2(\omega_T)}\big], \tag{1.7}$$

where ω_T denotes the patch of the element $T \in \mathcal{T}$.

The proof of the reliability makes use of the Helmholtz decomposition to deal with mixed boundary conditions. For the proof of the efficiency estimate, the non-avoidance of hanging nodes needs the extended definition of edge patches. We stress that [13] only treats the Dirichlet problem $\Gamma_D = \Gamma$ and that the a posteriori error analysis is restricted to the case of regular meshes. Therefore the definition of $\mathcal{I}u_h$ had to be substantially modified.

The content of this paper is organized as follows: In Section 2, we introduce the notation that is used below. In particular, we define the concept of an *almost regular triangulation*, which allows the analytical error analysis in case of certain hanging nodes. Section 3 gives a short summary on the classical cell-centered finite volume method for our model problem. We recall the ideas of the diamond path, where emphasis is laid on the treatment of nodes $a \in \Gamma_N$ that lie on the Neumann boundary Γ_N. In Section 4, we define the Morley interpolant and collect the orthogonality properties used for the error analysis. Reliability and efficiency of the error estimator η are then proven in Section 5. Numerical experiments, found in Section 6, confirm the theoretical results and conclude the work. In particular, we observe

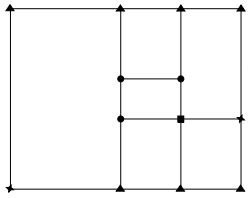

(a) Circles denote nodes in $\mathcal{N}_H$, squares denote nodes in $\mathcal{N}_F$, triangles denote nodes in $\mathcal{N}_D$, stars denote nodes in $\mathcal{N}_N$.

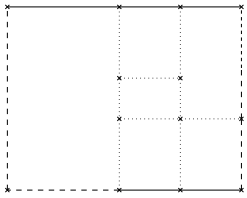

(b) Full lines denote edges in $\mathcal{E}_D$, dashed lines denote edges in $\mathcal{E}_N$, dotted lines denote edges in $\mathcal{E}_E$.

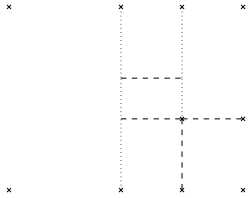

(c) Dotted lines denote edges in $\mathcal{E}_H$, dashed lines denote edges in $\mathcal{E}_0$.

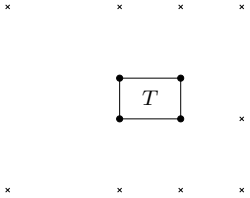

(d) Full lines denote edges in $\mathcal{E}_T$, circles denote nodes in $\mathcal{N}_T$.

FIGURE 2.1. *The sets of edges and nodes for a simple (almost regular) triangulations, which consists of* 6 *rectangular elements.*

that the proposed strategy even recovers the optimal order of convergence with respect to the energy norm $\|u - u_h\|_{1,h}$.

2. Preliminaries & Notations

In this section, we introduce the notation for the triangulations that are considered below. In particular, we define the so-called *almost regular* triangulation which allows certain hanging nodes.

2.1. Almost Regular Triangulation. Throughout, $\mathcal{T}$ denotes a triangulation of Ω, where $\mathcal{N}$ and $\mathcal{E}$ are the corresponding set of nodes and edges, respectively. We assume that the elements $T \in \mathcal{T}$ are triangles or rectangles, which are nondegenerate either. For $T \in \mathcal{T}$, $h_T := \operatorname{diam}(T)$ denotes the Euclidean diameter and ϱ_T is the corresponding height, i.e. the volume of T is $|T| = h_T \varrho_T$ in case T being a rectangle and $|T| = h_T \varrho_T/2$ in case T being a triangle. Moreover, for an edge $E \in \mathcal{E}$, we denote by h_E its length.

Nodes. In the following, we introduce a partition

$$\mathcal{N} = \mathcal{N}_D \cup \mathcal{N}_N \cup \mathcal{N}_H \cup \mathcal{N}_F$$

of $\mathcal{N}$ into Dirichlet and Neumann nodes, hanging nodes, and free nodes, respectively: First, let $\mathcal{N}_D := \big\{a \in \mathcal{N} \,\big|\, a \in \Gamma_D\big\}$ resp. $\mathcal{N}_N := \big\{a \in \mathcal{N} \,\big|\, a \in \Gamma_N\big\}$ be the set of all nodes that belong to the Dirichlet boundary resp. Neumann boundary. A node $a \in \mathcal{N}\backslash(\mathcal{N}_D \cup \mathcal{N}_N)$ is a hanging node provided that there are elements $T_1, T_2 \in \mathcal{T}$ such that $a \in T_1 \cap T_2$ is a node of T_1 but not of T_2. Let $\mathcal{N}_H$ be the set of all hanging nodes. Finally, the set of free nodes is $\mathcal{N}_F := \mathcal{N}\backslash(\mathcal{N}_D \cup \mathcal{N}_N \cup \mathcal{N}_H)$. For an element $T \in \mathcal{T}$, we denote with $\mathcal{N}_T$ the set of nodes of T, i.e. $|\mathcal{N}_T| = 3$ for T being a triangle and $|\mathcal{N}_T| = 4$ for T being a rectangle, respectively.

Edges. For the edges, we introduce a partition

$$\mathcal{E} = \mathcal{E}_D \cup \mathcal{E}_N \cup \mathcal{E}_H \cup \mathcal{E}_E$$

into Dirichlet and Neumann edges, non-elementary edges, and interior elementary edges, respectively: First, we define $\mathcal{E}_D := \big\{E \in \mathcal{E} \,\big|\, E \subseteq \Gamma_D\big\}$ and $\mathcal{E}_N := \big\{E \in \mathcal{E} \,\big|\, E \subseteq \overline{\Gamma}_N\big\}$. Second, an interior edge $E \in \mathcal{E}$ is non-elementary, if there are pairwise different nodes

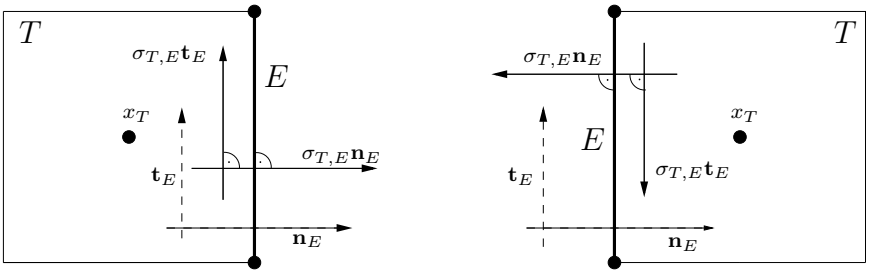

(a) $\sigma_{T,E} = 1$ (b) $\sigma_{T,E} = -1$

FIGURE 2.2. *The dashed lines show the a priori chosen normal vector $\mathbf{n}_E$ resp. tangential vector $\mathbf{t}_E$ on the edge E, whereas the full lines are the outer normal vector $\mathbf{n}_T|_E = \sigma_{T,E}\mathbf{n}_E$ of T resp. $\mathbf{t}_T|_E = \sigma_{T,E}\mathbf{t}_E$ with respect to the edge E.*

$x, y, z \in \mathcal{N}$ such that $E = \operatorname{conv}\{x, y\}$ and $z \in E$, i.e. there is a hanging node z in the interior of E. The set of all non-elementary edges is denoted by $\mathcal{E}_H$. Contrary, $\mathcal{E}\backslash\mathcal{E}_H$ denotes the set of all elementary edges, which is split into boundary edges $\mathcal{E}_D \cup \mathcal{E}_N$ and interior elementary edges $\mathcal{E}_E := \mathcal{E}\backslash(\mathcal{E}_H \cup \mathcal{E}_D \cup \mathcal{E}_N)$. Moreover, we define the set

$$\mathcal{E}_0 := \big\{E \in \mathcal{E}_E \,\big|\, \nexists E' \in \mathcal{E}_H \quad E \subsetneqq E'\big\},$$

of all interior elementary edges which are not part of a non-elementary edge. Finally, for an element $T \in \mathcal{T}$, we denote with $\mathcal{E}_T \subset \mathcal{E}$ the set of all edges of T, i.e.

$$\mathcal{E}_T := \big\{E \in \mathcal{E} \,\big|\, E \subseteq \partial T, \quad \nexists E' \in \mathcal{E} \quad E' \subsetneqq E\big\}.$$

Almost Regular Triangulations. We say that the triangulation $\mathcal{T}$ is almost regular, if

(i) the mixed boundary conditions are resolved, i.e. each edge $E \in \mathcal{E}$ with $E \cap \Gamma \neq \emptyset$ satisfies either $E \in \mathcal{E}_D$ or $E \in \mathcal{E}_N$,

(ii) the intersection $T_1 \cap T_2$ of two elements $T_1, T_2 \in \mathcal{T}$ with $T_1 \neq T_2$ is either empty or a node or an edge.

(iii) each non-elementary edge $E \in \mathcal{E}_H$ is the finite union of elementary edges, i.e. there are finitely many elementary edges $E_1, \dots, E_n \in \mathcal{E}_E$ such that $E = \bigcup_{i=1}^n E_i$.

With respect to regular triangulations in the sense of Ciarlet, the only difference is that in (ii) the intersection $T_1 \cap T_2$ may be, for instance, a node (or an edge) of T_1 but not of T_2, cf. Figure 2.1 above. However, in case of $E := T_1 \cap T_2$ being an edge, (iii) implies that there holds at least either $E \in \mathcal{E}_{T_1}$ or $E \in \mathcal{E}_{T_2}$. From now on, we assume that all triangulations are at least almost regular (or even regular).

2.2. Normal and Tangential Vectors. For each edge $E \in \mathcal{E}$, we fix a normal vector $\mathbf{n}_E$ as follows: For $E \in \mathcal{E}_D \cup \mathcal{E}_N$, let $\mathbf{n}_E$ point outwards of Ω. For an edge $E \in \mathcal{E}_H$, there is a unique element $T \in \mathcal{T}$ with $E \in \mathcal{E}_T$, and we choose $\mathbf{n}_E$ to point into T. For each elementary edge $E' \in \mathcal{E}_E$ with $E' \subset E$, we define $\mathbf{n}_{E'} := \mathbf{n}_E$. For the remaining edges, namely $E \in \mathcal{E}_0$, we may choose the orientation of $\mathbf{n}_E$ arbitrarily.

In Section 3, we shall use the following notational convention: For each elementary edge $E \in \mathcal{E}_E$, there are unique elements $T_{W,E}$ and $T_{E,E}$ such that $E \subseteq T_{W,E} \cap T_{E,E}$ and such that $\mathbf{n}_E$ points from $T_{W,E}$ to $T_{E,E}$ (i.e. from West to East). For $E \in \mathcal{E}_D \cup \mathcal{E}_N$, there is a unique element $T_{W,E}$ with $E \subset \partial T_{W,E}$. If the edge E is clear from the context, we omit the additional subscript and simply write, e.g., $T_W = T_{W,E}$.

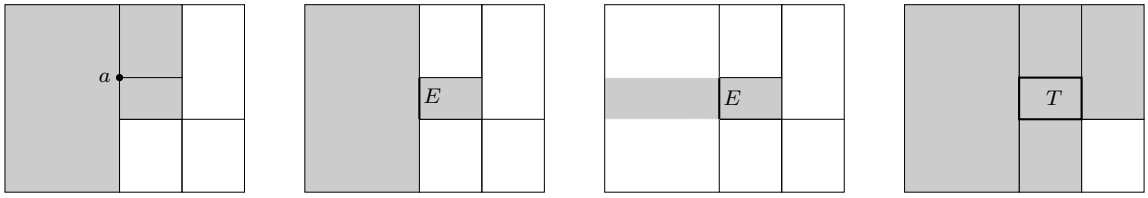

(a) ω_a (b) ω_E (c) ω_E^* (d) ω_T

FIGURE 2.3. *The four patches introduced in Section 2.3.*

Moreover, for each element $T \in \mathcal{T}$ and an edge $E \in \mathcal{E}$ with $E \subset \partial T$, we define the sign

$$\sigma_{T,E} = \begin{cases} +1, & \text{provided } T = T_{W,E}, \\ -1, & \text{else,} \end{cases} \tag{2.1}$$

i.e. $\sigma_{T,E}\mathbf{n}_E$ is the outer normal vector $\mathbf{n}_T|_E$ of T restricted to the edge E.

Finally, the tangential vector $\mathbf{t}_E$ of an edge $E \in \mathcal{E}$ is chosen orthogonal to $\mathbf{n}_E$ in mathematical positive sense. We note that $\sigma_{T,E}\mathbf{t}_E$ is the tangential vector $\mathbf{t}_T|_E$ of an element $T \in \mathcal{T}$ restricted to the edge E.

2.3. Patches. We recall the definition of the patches which are well-known from finite element analysis. Additionally, we introduce the elementary patch of an edge which is needed for the handling of the hanging nodes in our a posteriori error analysis.

Patch of a Node. For $a \in \mathcal{N}$, the patch is given by

$$\omega_a = \bigcup_{T \in \widetilde{\omega}_a} T, \quad \text{where} \quad \widetilde{\omega}_a := \big\{T \in \mathcal{T} \,\big|\, a \subseteq \partial T\big\}.$$

Patch of an Edge. For an elementary edge $E \in \mathcal{E}\backslash\mathcal{E}_H$, the patch is given by

$$\omega_E := \bigcup_{T \in \widetilde{\omega}_E} T, \quad \text{where} \quad \widetilde{\omega}_E := \big\{T \in \mathcal{T} \,\big|\, E \subseteq \partial T\big\}.$$

For a non-elementary edge $E \in \mathcal{E}_H$ and $E_1, \dots, E_n \in \mathcal{E}^*$ with $E = \bigcup_{i=1}^n E_i$, we define

$$\omega_E := \bigcup_{T \in \widetilde{\omega}_E} T = \bigcup_{i=1}^n \omega_{E_i}, \quad \text{where} \quad \widetilde{\omega}_E := \bigcup_{i=1}^n \widetilde{\omega}_{E_i}.$$

Elementary Patch of an Edge. Let us consider a non-elementary edge $E \in \mathcal{E}_H$ and $E_1, \dots, E_n \in \mathcal{E}^*$ with $E = \bigcup_{i=1}^n E_i$. Then, there is a unique element $T_E \in \mathcal{T}$ with $E \in \mathcal{E}_{T_E}$. Moreover, there are unique elements $T_i \in \mathcal{T}$ such that $E_i \in \mathcal{E}_{T_i}$. We denote by $a_1, \dots, a_{n-1} \in \mathcal{N}_H$ the hanging nodes, which are on E. Moreover, let a_0 and a_n be the nodes of E. Without loss of generality, a_{i-1}, a_i are the nodes of E_i, i.e.

$$E_i = \operatorname{conv}\{a_{i-1}, a_i\}.$$

If $T_E = \operatorname{conv}\{a_0, a_n, b\}$ is a triangle, we define triangles $\widetilde{T}_i := \operatorname{conv}\{a_{i-1}, a_i, b\}$ and note that

$$T_E = \bigcup_{i=1}^n \widetilde{T}_i \quad \text{and} \quad \operatorname{int}(\widetilde{T}_i) \cap \operatorname{int}(\widetilde{T}_j) = \emptyset \quad \text{for } i \neq j, \tag{2.2}$$

where int(·) denotes the topological interior of a set. We stress that the triangles $\widetilde{T}_i$ cannot be elements of the triangulation $\mathcal{T}$. For T_E a rectangle, we can construct rectangles $\widetilde{T}_i$ with (2.2). For each of the elementary edges E_i, we may then define the elementary patch

$$\omega^*_{E_i} := T_i \cup \widetilde{T}_i \quad \text{and} \quad \widetilde{\omega}^*_{E_i} := \{T_i, \widetilde{T}_i\}.$$

So far, we have defined the patch ω^*_E for all edges $E \in \mathcal{E}$ which are contained in a non-elementary edge. For the remaining edges $E \in \mathcal{E}$, we define $\omega^*_E := \omega_E$ and $\widetilde{\omega}^*_E := \widetilde{\omega}_E$.

Patch of an Element. The patch of an element $T \in \mathcal{T}$ is defined by

$$\omega_T := \bigcup_{T \in \widetilde{\omega}_T} T, \quad \text{where} \quad \widetilde{\omega}_T := \big\{T' \in \mathcal{T} \,\big|\, T \cap T' \in \mathcal{E}\big\}.$$

2.4. Jump Terms. For $T \in \mathcal{T}$, $E \subseteq \partial T$, and $\varphi \in H^1(T)$, let $\varphi|_{E,T}$ denote the trace of φ on E. Now, let $E \in \mathcal{E}_E$ be an interior elementary edge and T_E and T_W the unique elements with $E = T_E \cap T_W$. For a $\{T_E, T_W\}$-piecewise H^1 function φ, the jump of φ on E is defined by

$$[\![\varphi]\!]_E := \varphi|_{E,T_E} - \varphi|_{E,T_W}. \tag{2.3}$$

Note that $[\![\varphi]\!]_E = 0$ provided $\varphi \in H^1(T_E \cup T_W)$. Moreover, for a $\{T_E, T_W\}$-piecewise polynomial φ, the jump on E reads

$$[\![\varphi]\!]_E(x) := \lim_{t \to 0_+} \varphi(x + t\mathbf{n}_E) - \lim_{t \to 0_+} \varphi(x - t\mathbf{n}_E) \quad \text{for all } x \in E. \tag{2.4}$$

For each non-elementary edge $E \in \mathcal{E}_H$, we define the jump $[\![\varphi]\!]_E$ by

$$[\![\varphi]\!]_E(x) := [\![\varphi]\!]_{E_i}(x) \quad \text{for all } x \in E_i,$$

where $E = \bigcup_{i=1}^n E_i$ with $E_1, \dots, E_n \in \mathcal{E}_E$.

3. Cell-Centered Finite Volume Method

This section summarizes the discretization for the cell-centered Finite Volume Method for our model problem. It specially points out the difference between the approximation of the diffusive flux on an admissible mesh and an almost regular mesh.

3.1. Discretization Ansatz. We integrate the strong form (1.1) over a control volume $T \in \mathcal{T}$ and use the Gauss divergence theorem to obtain

$$\int_T f \, dx = -\int_T \Delta u \, dx = -\int_{\partial T} \frac{\partial u}{\partial \mathbf{n}_T} \, ds = -\sum_{E \in \mathcal{E}_T} \sigma_{T,E} \int_E \frac{\partial u}{\partial \mathbf{n}_E} \, ds \quad \text{for all } T \in \mathcal{T}. \tag{3.1}$$

With the diffusive flux $\Phi^D_E(u) = \int_E \partial u / \partial \mathbf{n}_E \, ds$, we get the so-called balance equation

$$-\sum_{E \in \mathcal{E}_T} \sigma_{T,E} \Phi^D_E(u) = \int_T f \, dx \quad \text{for all } T \in \mathcal{T}. \tag{3.2}$$

For the cell-centered finite volume method, one replaces the continuous diffusion flux $\Phi^D_E(u)$ by a discrete diffusion flux $F^D_E(u_h)$, which is discussed in Section 3.2. Here, $u_h \in \mathcal{P}^0(\mathcal{T})$ is a

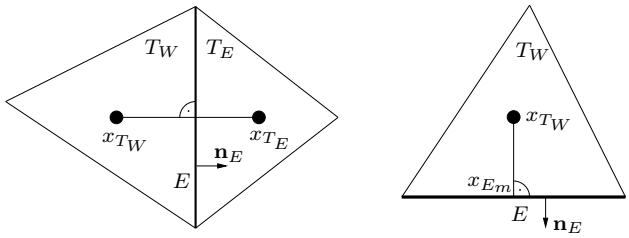

FIGURE 3.1. *The orthogonality condition for $E \in \mathcal{E}_E$ (left) resp. $E \in \mathcal{E}_D$ (right) for an admissible mesh in the sense of* [11].

piecewise constant approximation of u, namely $u_T := u_h|_T \approx u(x_T)$, where x_T denotes the center of an element $T \in \mathcal{T}$. The discrete problem thus reads: Find $u_h \in \mathcal{P}^0(\mathcal{T})$ such that

$$-\sum_{E\in\mathcal{E}_T} \sigma_{T,E} F_E^D(u_h) = \int_T f\,dx, \quad \text{for all } T \in \mathcal{T}. \tag{3.3}$$

3.2. Discretization of Diffusion Flux. Note that $\Phi_E^D(u_h) = \int_E g\,ds$ is known for a Neumann edge $E \in \mathcal{E}_N$. One therefore defines

$$F_E^D(u_h) := \Phi_E^D(u_h) = \int_E g\,ds \quad \text{for } E \in \mathcal{E}_N. \tag{3.4}$$

Moreover, for a non-elementary edge with $E = \bigcup_{i=1}^n E_i$ and $E_i \in \mathcal{E}_E$, there holds $\Phi_E^D(u) = \sum_{i=1}^n \Phi_{E_i}^D(u)$, which leads to the definition

$$F_E^D(u_h) := \sum_{i=1}^n F_{E_i}^D(u_h) \quad \text{for all} \quad E_1,\dots,E_n \in \mathcal{E}_E \text{ and } E = \bigcup_{i=1}^n E_i \in \mathcal{E}_H. \tag{3.5}$$

Therefore, it only remains to define $F_E^D(u_h)$ for $E \in \mathcal{E}_E \cup \mathcal{E}_D$.

Admissible Meshes. For an admissible mesh in the sense of [11, Definition 9.1], a first order difference scheme leads to

$$\Phi_E^D(u) \approx F_E^D(u_h) := \begin{cases} \dfrac{u_{T_E} - u_{T_W}}{|x_{T_E} - x_{T_W}|}\, h_E, & \text{if } E \in \mathcal{E}_E \text{ and } E = T_W \cap T_E, \\[2ex] \dfrac{u_{E_m} - u_{T_W}}{|x_{E_m} - x_{T_W}|}\, h_E, & \text{if } E \in \mathcal{E}_D \text{ and } E = T_W \cap \Gamma_D, \end{cases} \tag{3.6}$$

with $u_{T_W} = u_h|_{T_W} \approx u(x_{T_W})$ and $u_{T_E} \approx u(x_{T_E})$ as well as, for $E \in \mathcal{E}_D$, $u_{E_m} \approx u_D(x_{E_m})$.

The admissibility of the mesh $\mathcal{T}$ allows to choose the centers x_T for $T \in \mathcal{T}$ in a way that the edges $E = T_W \cap T_E$ for any $T_W, T_E \in \mathcal{T}$ are orthogonal to the directions $x_{T_E} - x_{T_W}$, cf. Figure 3.1. For general meshes, it is not possible to choose the centers x_T appropriately, and the approximation (3.6) is not consistent [11].

***Remark* 3.1.** Even if a triangular mesh is admissible in the sense of [11, Definition 9.1], local mesh-refinement is nontrivial: One has to guarantee that all angles are strictly less than $\pi/2$, i.e. one cannot avoid remeshing of the domain. For rectangular meshes, local mesh-refinement cannot avoid hanging nodes. This, however, contradicts the admissibility condition.

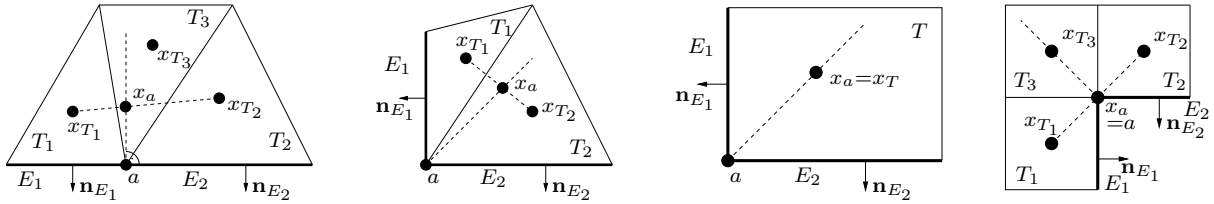

FIGURE 3.2. *The different cases for calculating u_a with $a \in \mathcal{N}_N$ and $E_1, E_2 \in \mathcal{E}_N$.*

Diamond Path Method. A possible choice of $F_E^D(u_h)$ for general meshes is the so-called *diamond path method*, which has been mathematically analyzed in [8, 9] for rectangular meshes with maximum one hanging node per edge. For each node $a \in \mathcal{N}$, we define

$$u_a = \begin{cases} \displaystyle\sum_{T \in \widetilde{\omega}_a} \psi_T(a)\, u_T, & \text{for all } a \in \mathcal{N}_F \cup \mathcal{N}_H, \\ u_D(a), & \text{for all } a \in \mathcal{N}_D, \\ \overline{u}_a + \overline{g}_a, & \text{for all } a \in \mathcal{N}_N, \end{cases} \tag{3.7}$$

for certain weights $\big\{\psi_T(a) \,\big|\, T \in \mathcal{T}, a \in \mathcal{N}_T\big\}$. For details on the computation of the weights, the reader is referred to [7, 8, 9, 10]. We stress, that the computation can be done in linear complexity with respect to the number $\#\mathcal{T}$ of elements.

We only remark on the computation of $\overline{u}_a$ and $\overline{g}_a$ in case of a Neumann node $a \in \mathcal{N}_N$, cf. Figure 3.2: To $a \in \mathcal{N}_N$ correspond two edges $E_1, E_2 \in \mathcal{E}_N$ such that $\{a\} = E_1 \cap E_2$. Let $\mathbf{n}_j$ denote the normal vector of E_j. In case of $\#\widetilde{\omega}_a > 1$, let $T_1, T_2 \in \widetilde{\omega}_a$ with $T_1 \neq T_2$. We define x_a as the intersection of the line $\gamma_1(s) = a + s(\mathbf{n}_1 + \mathbf{n}_2)/2$ and the line $\gamma_2(t) = t(x_{T_1} - x_{T_2})$. Moreover, provided $\#\widetilde{\omega}_a > 2$, we assume that $|x_a - a|$ is minimized over all pairs $T_1, T_2 \in \widetilde{\omega}_a$. Then, $\overline{u}_a \approx u(x_a)$ is interpolated linearly from u_{T_1} and u_{T_2},

$$\overline{u}_a = \frac{u_{T_2} - u_{T_1}}{|x_{T_2} - x_{T_1}|} |x_a - x_{T_1}| + u_{T_1}.$$

For $\mathbf{n}_1 = \mathbf{n}_2$, we choose

$$\overline{g}_a = |x_a - a| \Big(\frac{1}{|E_1|} \int_{E_1} g \, ds + \frac{1}{|E_2|} \int_{E_2} g \, ds \Big) / 2$$

and finally, for $\mathbf{n}_1 \neq \mathbf{n}_2$, we choose

$$\overline{g}_a = \lambda \frac{1}{|E_1|} \int_{E_1} g \, ds + \mu \frac{1}{|E_2|} \int_{E_2} g \, ds,$$

where $\lambda, \mu \in \mathbb{R}$ are calculated from the linear equation $a - x_a = \lambda \mathbf{n}_1 + \mu \mathbf{n}_2$. In case $\widetilde{\omega}_a = \{T\}$, i.e. a is the node of only one element $T \in \mathcal{T}$, we choose $x_a = x_T$ and $\overline{u}_a = u_T$ whereas $\overline{g}_a$ is computed as before.

***Remark* 3.2.** Provided $x_a = a$, we obtain $a - x_a = 0$, $\lambda = \mu = 0$, and $\overline{g}_a = 0$.

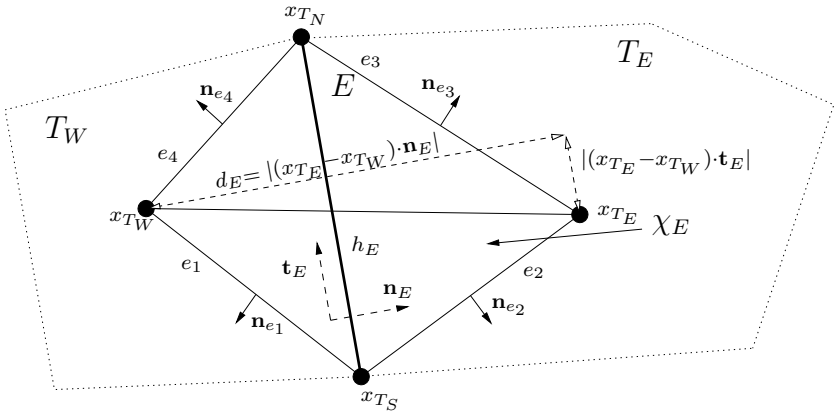

FIGURE 3.3. *Diamond Path with domain χ_E.*

With the notations from Figure 3.3, where x_{T_S} and x_{T_N} are the starting and end point of $E \in \mathcal{E}_E \cup \mathcal{E}_D$, we compute $F_E^D(u_h)$. For an elementary edge $E \in \mathcal{E}_E$

$$
\begin{aligned}
F_E^D(u_h) &:= h_E \left(\frac{u_{T_E} - u_{T_W}}{d_E} - \alpha_E \frac{u_{T_N} - u_{T_S}}{h_E} \right) \\
&\text{with} \qquad \alpha_E = \frac{(x_{T_E} - x_{T_W}) \cdot \mathbf{t}_E}{(x_{T_E} - x_{T_W}) \cdot \mathbf{n}_E}, \qquad d_E = (x_{T_E} - x_{T_W}) \cdot \mathbf{n}_E.
\end{aligned} \tag{3.8}
$$

Here, the additional unknowns u_{T_N} and u_{T_S} are located at the nodes x_{T_N} and x_{T_S} and are computed by (3.7). For a boundary edge $E \in \mathcal{E}_D$, we compute $F_E^D(u_h)$ by (3.8), where x_{T_E} is now replaced by the midpoint x_{E_m} of E and u_{T_E} becomes $u_D(x_{E_m})$.

4. Morley Interpolant

Let $u_h \in \mathcal{P}^0(\mathcal{T})$ be the computed discrete solution. In this section, we define an interpolant $\mathcal{I}u_h$ which is appropriate for the a posteriori error analysis. The definition of which is an extension of the definition in [13, Section 5] to the case of hanging nodes and Neumann nodes.

Triangular Morley Element. Let $T = \operatorname{conv}\{a_1, a_2, a_3\} \subset \mathbb{R}^2$ be a non-degenerate triangle with edges $E_j = \operatorname{conv}\{a_j, a_{j+1}\}$, where $a_4 := a_1$. The standard Morley element $(T, \mathcal{P}_T, \Sigma_T)$ is given by $\mathcal{P}_T = \mathcal{P}_2$ and $\Sigma_T = (S_1, \dots, S_6)$, where

$$
S_j(p) = p(a_j) \quad \text{and} \quad S_{j+3}(p) = \int_{E_j} \frac{\partial p}{\partial \mathbf{n}_{T,E_j}}\, ds \quad \text{for } j = 1, \dots, 3 \text{ and } p \in \mathcal{P}_2. \tag{4.1}
$$

Note that $S_{j+3}(p) = h_{E_j} \partial p(m_j)/\partial \mathbf{n}_{T,E_j}$, where $m_j := (a_j + a_{j+1})/2$ denotes the midpoint of E_j, so that this definition is consistent with [4, Section 8.3].

Rectangular Morley Element. Let $T = \operatorname{conv}\{a_1, a_2, a_3, a_4\} \subset \mathbb{R}^2$ be a non-degenerate rectangle with edges E_j. A Morley-type element $(T, \mathcal{P}_T, \Sigma_T)$ is then given by $\mathcal{P}_T = \mathcal{P}_2 \oplus \operatorname{span}\{x^3 - 3xy^2, y^3 - 3yx^2\}$ and $\Sigma_T = (S_1, \dots, S_8)$, where

$$
S_j(p) = p(a_j) \quad \text{and} \quad S_{j+4}(p) = \int_{E_j} \frac{\partial p}{\partial \mathbf{n}_{T,E_j}}\, ds \quad \text{for } j = 1, \dots, 4 \text{ and } p \in \mathcal{P}, \tag{4.2}
$$

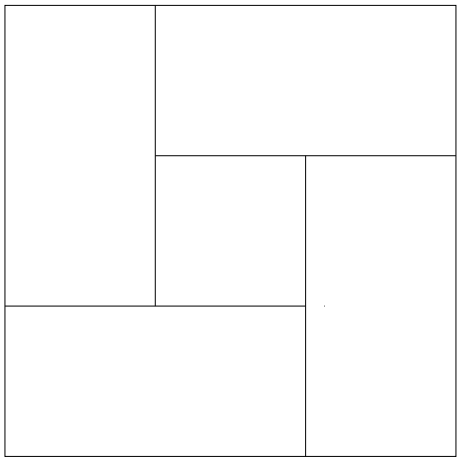

FIGURE 4.1. *An almost regular triangulation, where the elementwise and recursive computation of $\mathcal{I}u_h$ does not stop.*

cf. [13, Section 4.2]. Note that the polynomials $x^3 - 3xy^2$ and $y^3 - 3yx^2$, which enrich the ansatz space, are harmonic.

The Morley Interpolant. In either of the cases, that T is a non-degenerate triangle or rectangle, the Morley element $(T, \mathcal{P}_T, \Sigma_T)$ is a nonconforming finite element. The Morley interpolant $\mathcal{I}u_h$ satisfies elementwise $(\mathcal{I}u_h)|_T \in \mathcal{P}_T$ for all $T \in \mathcal{T}$ defined by the following properties (4.3)–(4.5): For each free node $a \in \mathcal{N}_T \cap \mathcal{N}_F$, the value $\mathcal{I}u_h(a)$ satisfies

$$(\mathcal{I}u_h)|_T(a) = \sum_{T_a \in \widetilde{\omega}_a} \psi_{T_a}(a) u_h|_{T_a}. \tag{4.3}$$

where the weights $\psi_{T_a}(a)$ are the same as for the computation of u_h by use of the diamond cell method. For each boundary node, the value $\mathcal{I}u_h(a)$ is prescribed

$$(\mathcal{I}u_h)|_T(a) = \begin{cases} u_D(a) & \text{for } a \in \mathcal{N}_T \cap \mathcal{N}_D, \\ \overline{u}_a + \overline{g}_a & \text{for } a \in \mathcal{N}_T \cap \mathcal{N}_N, \end{cases} \tag{4.4}$$

where the calculation of $\overline{u}_a$ and $\overline{g}_a$ was discussed in Section 3. For each hanging node $a \in \mathcal{N}_T \cap \mathcal{N}_H$, there holds

$$(\mathcal{I}u_h)|_T(a) = (\mathcal{I}u_h)|_{T_a}(a), \tag{4.5}$$

where $T_a \in \mathcal{T}$ is the unique element with $a \in \operatorname{int}(E)$ for some (non-elementary) edge $E \in \mathcal{E}_{T_a}$. For each edge $E \in \mathcal{E}_T$ holds

$$\int_E \frac{\partial (\mathcal{I}u_h)|_T}{\partial \mathbf{n}_E} \, ds = F_E^D(u_h), \tag{4.6}$$

where $F_E^D(u_h)$ is the numerical flux from Section 3.2.

Lemma 4.1. *The Morley interpolant $\mathcal{I}u_h$ is uniquely defined by* (4.3)–(4.6)*. Moreover, $\mathcal{I}u_h$ is continuous in all nodes $a \in \mathcal{N}$ but not globally continuous in Ω.*

Proof. For an element $T \in \mathcal{T}$ without hanging nodes, i.e. $\mathcal{N}_T \cap \mathcal{N}_H = \emptyset$, the interpolant $(\mathcal{I}u_h)|_T$ is uniquely defined by (4.3)–(4.5) and (4.6) since $(T, \mathcal{P}_T, \Sigma_T)$ is a finite element. □

***Remark* 4.1.** The computation of $\mathcal{I}u_h$ can be performed by solving a large system of linear equations which is coupled through the hanging nodes. However, normally $\mathcal{I}u_h$ can be computed locally by solving a 6×6 (resp. 8×8) system for each element $T \in \mathcal{T}$. For an element $T \in \mathcal{T}$ without hanging nodes, the interpolant $(\mathcal{I}u_h)|_T$ is uniquely determined by (4.3)–(4.4) and (4.6). For an element with hanging nodes, we have to compute $(\mathcal{I}u_h)|_{T_a}$ first, cf. (4.5). This leads to a recursive algorithm. Figure 4.1 shows an almost regular triangulation, where the proposed recursion would not stop. Instead, one has to solve a global linear system to compute $\mathcal{I}u_h$.

Properties of Morley Interpolant. From the definition of the discrete scheme and the property (4.5), we obtain an additional orthogonality property of $\mathcal{I}u_h$.

Lemma 4.2. *The residual $R := f + \Delta(\mathcal{I}u_h)$ is L^2-orthogonal to $\mathcal{P}^0(\mathcal{T})$, i.e.*

$$\int_T \big(f + \Delta(\mathcal{I}u_h)\big)\, dx = 0 \quad \text{for all } T \in \mathcal{T}. \tag{4.7}$$

In particular, the residual satisfies $R = f - f_{\mathcal{T}}$.

Proof. From integration by parts and the definition of the balance equation (3.2), we infer

$$\int_T \Delta(\mathcal{I}u_h)|_T\, dx = \int_{\partial T} \frac{\partial(\mathcal{I}u_h)|_T}{\partial \mathbf{n}_T}\, ds = \sum_{E \in \mathcal{E}_T} \sigma_{T,E} F_E^D(u_h) = -\int_T f(x)\, dx,$$

where we have used (4.6) in the second equality. In particular, there holds $R_{\mathcal{T}}|_T := |T|^{-1} \int_T R\, dx = 0$. With $\Delta_{\mathcal{T}}(\mathcal{I}u_h) \in \mathcal{P}^0(\mathcal{T})$, we obtain $R = R - R_{\mathcal{T}} = f - f_{\mathcal{T}}$. □

According to the definition of $\mathcal{I}u_h$ on the Dirichlet and Neumann boundary, namely (4.4) and (4.5), we obtain corresponding orthogonalities.

Lemma 4.3. *For boundary edges hold*

$$\int_E \frac{\partial(u - \mathcal{I}u_h)}{\partial \mathbf{t}_E}\, ds = 0 \quad \text{for all } E \in \mathcal{E}_D \tag{4.8}$$

as well as

$$\int_E \frac{\partial(u - \mathcal{I}u_h)}{\partial \mathbf{n}_E}\, ds = 0 \quad \text{for all } E \in \mathcal{E}_N. \tag{4.9}$$

Proof. For $E \in \mathcal{E}_D$, let a_S and a_N be the starting and end point of E, respectively. Then,

$$\int_E \frac{\partial(u - \mathcal{I}u_h)}{\partial \mathbf{t}_E}\, ds = (u - \mathcal{I}u_h)(a_N) - (u - \mathcal{I}u_h)(a_S) = 0$$

by use of (4.4). To prove (4.9), we use (4.6) and the definition of the finite volume scheme:

$$\int_E \frac{\partial(\mathcal{I}u_h)}{\partial \mathbf{n}_E}\, ds = F_E^D(u_h) = \int_E g\, ds,$$

where $g = \partial u / \partial \mathbf{n}$. □

Finally, we note some orthogonality relations of the normal and tangential jumps of $\mathcal{I}u_h$ which follow again from (4.6) [in combination with (3.5)] and from the nodal values (4.3)–(4.5) of $\mathcal{I}u_h$.

Lemma 4.4. *For the interior edges hold*

$$\int_E \left[\!\!\left[\frac{\partial(\mathcal{I}u_h)}{\partial \mathbf{n}_E} \right]\!\!\right] ds = 0 \quad \text{for all } E \in \mathcal{E}_0 \cup \mathcal{E}_H \tag{4.10}$$

as well as

$$\int_E \left[\!\!\left[\frac{\partial(\mathcal{I}u_h)}{\partial \mathbf{t}_E} \right]\!\!\right] ds = 0 \quad \text{for all } E \in \mathcal{E}_E \tag{4.11}$$

Proof. We first prove (4.10) for $E \in \mathcal{E}_H$. There holds $E = \bigcup_{i=1}^n E_i$ with $E_1, \dots, E_n \in \mathcal{E}^*$, $E_i = T_{W_i} \cap T_E$ and $\mathbf{n}_E$ shows from element T_{W_i} to T_E. Therefore, the definition (3.5) of the discrete flux on non-elementary edges implies

$$\int_E \left[\!\!\left[\frac{\partial(\mathcal{I}u_h)}{\partial \mathbf{n}_E} \right]\!\!\right] ds = \int_E \frac{\partial(\mathcal{I}u_h)|_{T_E}}{\partial \mathbf{n}_E}\, ds - \sum_{i=1}^n \int_{E_i} \frac{\partial(\mathcal{I}u_h)|_{T_{W_i}}}{\partial \mathbf{n}_E}\, ds = F_E(u_h) - \sum_{i=1}^n F_{E_i}(u_h) = 0.$$

For $E \in \mathcal{E}_0$, the proof of (4.10) works analogously with $n = 1$. To prove (4.11), let a_S and a_N be the starting and end point of $E \in \mathcal{E}_E$, respectively. Note that $[\![\mathcal{I}u_h]\!]_E(a_N) = 0 = [\![\mathcal{I}u_h]\!]_E(a_S)$ because of the continuity of $\mathcal{I}u_h$ in all nodes. Therefore,

$$\int_E \left[\!\!\left[\frac{\partial(\mathcal{I}u_h)}{\partial \mathbf{t}_E} \right]\!\!\right] ds = \int_{a_S}^{a_N} \left[\!\!\left[\frac{\partial(\mathcal{I}u_h)}{\partial \mathbf{t}_E} \right]\!\!\right] ds = [\![\mathcal{I}u_h]\!]_E(a_N) - [\![\mathcal{I}u_h]\!]_E(a_S) = 0,$$

which concludes the proof. □

5. A Posteriori Error Estimate

In this section, we provide a residual-based a posteriori error analysis for the error $u - \mathcal{I}u_h$, where $\mathcal{I}$ denotes the Morley interpolant from Section 4. The idea goes back to [13] and is now extended to almost regular triangulations and mixed boundary conditions. The mathematical techniques follow the a posteriori error analysis for nonconforming finite elements. Throughout, $\nabla_{\mathcal{T}}$ and $\Delta_{\mathcal{T}}$ denote the $\mathcal{T}$-piecewise gradient and Laplacian, respectively.

5.1. Residual-Based Error Estimator. For each element $T \in \mathcal{T}$, we define the refinement indicator

$$\begin{aligned} \eta_T^2 := h_T^2 \|f - f_{\mathcal{T}}\|_{L^2(T)}^2 &+ \sum_{E \in \mathcal{E}_T \cap \mathcal{E}_E} h_E^* \|[\![\nabla_{\mathcal{T}}(\mathcal{I}u_h)]\!]\|_{L^2(E)}^2 \\ &+ \sum_{E \in \mathcal{E}_T \cap \mathcal{E}_N} h_E \left\| \frac{\partial(u - \mathcal{I}u_h)}{\partial \mathbf{n}_E} \right\|_{L^2(E)}^2 + \sum_{E \in \mathcal{E}_T \cap \mathcal{E}_D} h_E \left\| \frac{\partial(u - \mathcal{I}u_h)}{\partial \mathbf{t}_E} \right\|_{L^2(E)}^2. \end{aligned} \tag{5.1}$$

Here, $f_{\mathcal{T}}$ denotes the $\mathcal{T}$-piecewise integral mean, i.e. $f_{\mathcal{T}}|_T := |T|^{-1} \int_T f\, dx$. Moreover, the length h_E^* of an edge $E \in \mathcal{E}^*$ is defined by

$$h_E^* := \begin{cases} h_{E'} & \text{if } E \subset E' \text{ for some } E' \in \mathcal{E}_H, \\ h_E, & \text{else, i.e. } E \in \mathcal{E}_0. \end{cases} \tag{5.2}$$

The residual-based error estimator is then given by the ℓ_2-sum $\eta = \big(\sum_{T \in \mathcal{T}} \eta_T^2\big)^{1/2}$ of all refinement indicators. In the following sections, we prove that η is (up to terms of higher order) a lower and upper bound of the error $\|\nabla_{\mathcal{T}}(u - \mathcal{I}u_h)\|_{L^2(\Omega)}$ in the energy norm.

5.2. Helmholtz Decomposition. To treat mixed boundary conditions instead of homogeneous Dirichlet conditions only, we need an improved Helmholtz decomposition which is recalled for the convenience of the reader. This decomposition is used for the reliability estimate of Section 5.3 only.

Theorem 5.1 ([12, Theorem 3.1])**.** *A function $\Phi \in L^2(\Omega)^2$ satisfies*

$$\operatorname{div} \Phi = 0 \quad \text{and} \quad \int_{\Gamma_j} \Phi \cdot \mathbf{n}\, ds = 0 \quad \text{for all connectedness components } \Gamma_j \text{ of } \Gamma, \tag{5.3}$$

if and only if there is a function $w \in H^1(\Omega)$ such that $\Phi = \operatorname{curl} w$. □

Corollary 5.2. *Given $\Phi \in L^2(\Omega)^2$, there are $v, w \in H^1(\Omega)$ with $\Phi = \nabla v + \operatorname{curl} w$ such that $v|_{\Gamma_D} = 0$ as well as $w|_{\Gamma_N} = 0$. In particular, there holds*

$$\|\Phi\|^2_{L^2(\Omega)} = \|\nabla v\|^2_{L^2(\Omega)} + \|\operatorname{curl} w\|^2_{L^2(\Omega)}. \tag{5.4}$$

Proof. There is a unique $v \in H^1_D(\Omega)$ such that

$$\int_\Omega \nabla v \cdot \nabla \phi\, dx = \int_\Omega \Phi \cdot \nabla \phi\, dx \quad \text{for all } \phi \in H^1_D(\Omega).$$

In particular, $\Psi := \Phi - \nabla v$ satisfies $\Psi \in H(\operatorname{div}; \Omega)$ with $\operatorname{div} \Psi = 0$ and, moreover,

$$\int_{\Gamma_N} \Psi \cdot \mathbf{n}\, \phi\, ds = \int_\Omega \Psi \cdot \nabla \phi\, dx = 0 \quad \text{for all } \phi \in H^1_D(\Omega),$$

whence $\Psi \cdot \mathbf{n}|_{\Gamma_N} = 0$ almost everywhere. Moreover, the Gauss divergence theorem proves

$$\int_{\Gamma_D} \Psi \cdot \mathbf{n}\, ds = \int_\Omega \operatorname{div} \Psi\, dx = 0.$$

Recall that $\Gamma = \Gamma_D \cup \Gamma_N$ and the assumption that Γ_D and Γ_N are connected. Thus, we may apply Theorem 5.1, which provides $w \in H^1(\Omega)$ with $\operatorname{curl} w = \Psi = \Phi - \nabla v$. Note that $0 = \operatorname{curl} w \cdot \mathbf{n} = \partial w / \partial \mathbf{t}$ on Γ_N. Since Γ_N is connected, we infer that w is constant on Γ_N. Subtracting a constant, we may therefore guarantee $w|_{\Gamma_N} = 0$. Finally, an integration by parts yields

$$\int_\Omega \nabla v \cdot \operatorname{curl} w\, dx = -\int_\Gamma \frac{\partial v}{\partial \mathbf{t}}\, w\, ds = 0,$$

i.e. ∇v and $\operatorname{curl} w$ are L^2-orthogonal. □

5.3. Reliability of Error Estimator.

Theorem 5.3. *There is a constant $c_1 > 0$ which depends only on the shape of the elements in $\mathcal{T}$ but neither on the size nor the number of elements such that*

$$\|\nabla_{\mathcal{T}}(u - \mathcal{I} u_h)\|_{L^2(\Omega)} \le c_1 \Big(\sum_{T \in \mathcal{T}} \eta_T^2 \Big)^{1/2}. \tag{5.5}$$

Proof. To abbreviate notation, we use the symbol $\lesssim$ if an estimate holds up to a multiplicative constant that depends only on the shape of the elements in $\mathcal{T}$. For $e := u - \mathcal{I} u_h$, the Helmholtz decomposition from Corollary 5.2 provides $v \in H^1(\Omega)$ and $w \in H^1(\Omega)$ such that

$$\nabla_{\mathcal{T}} e = \nabla v + \operatorname{curl} w \quad \text{and} \quad v|_{\Gamma_D} = 0 \quad \text{as well as} \quad w|_{\Gamma_N} = 0. \tag{5.6}$$

Moreover, there holds

$$\|\nabla v\|^2_{L^2(\Omega)} + \|\operatorname{curl} w\|^2_{L^2(\Omega)} = \|\nabla_{\mathcal{T}} e\|^2_{L^2(\Omega)} = \int_\Omega \nabla_{\mathcal{T}} e \cdot \nabla v \, dx + \int_\Omega \nabla_{\mathcal{T}} e \cdot \operatorname{curl} w \, dx. \tag{5.7}$$

We now estimate the two addends on the right-hand side separately. The first term reads

$$\int_\Omega \nabla_{\mathcal{T}} e \cdot \nabla v \, dx = \sum_{T\in\mathcal{T}} \int_T Rv \, dx + \int_{\Gamma_N} gv \, ds - \sum_{T\in\mathcal{T}} \int_{\partial T} \frac{\partial(\mathcal{I}u_h)}{\partial \mathbf{n}_T} \, v \, ds$$

according to elementwise integration by parts and the definition of the residual $R := f + \Delta_{\mathcal{T}}(\mathcal{I}u_h)$. We now consider the sum over the boundary integrals, namely

$$\sum_{T\in\mathcal{T}} \int_{\partial T} \frac{\partial(\mathcal{I}u_h)}{\partial \mathbf{n}_T} \, v \, ds = \sum_{T\in\mathcal{T}} \sum_{E\in\mathcal{E}_T} \sigma_{T,E} \int_E \frac{\partial(\mathcal{I}u_h)}{\partial \mathbf{n}_E} \, v \, ds.$$

For $E \in \mathcal{E}_D$, the boundary integral vanishes due to $v|_{\Gamma_D} = 0$. The Neumann edges $E \in \mathcal{E}_N$ are combined with the boundary integral $\int_{\Gamma_N} g \, ds$. Each edge $E \in \mathcal{E}_0$ appears twice for associated elements T_W and T_E, respectively. The normal vectors $\sigma_{T_W,E}\, \mathbf{n}_E$ and $\sigma_{T_E,E}\, \mathbf{n}_E$ only differ in the sign so that we obtain the jump of the normal derivative on E. For a non-elementary edge $E \in \mathcal{E}_H$ with $E = \bigcup_{i=1}^n E_i$ and $E_i \in \mathcal{E}_E$, both, E as well as the elementary edges E_i appear only once in the sum. Similarly to the prior arguments we are led to the jump of the normal derivative on E, where we make use of $\mathbf{n}_E = -\mathbf{n}_{E_i}$ for all $i = 1, \dots, n$. Altogether, we obtain

$$\int_\Omega \nabla_{\mathcal{T}} e \cdot \nabla v \, dx = \sum_{T\in\mathcal{T}} \int_T Rv \, dx - \sum_{E\in\mathcal{E}_0\cup\mathcal{E}_H} \int_E \Big[\!\Big[\frac{\partial(\mathcal{I}u_h)}{\partial \mathbf{n}_E} \Big]\!\Big] v \, ds + \sum_{E\in\mathcal{E}_N} \int_E \Big(g - \frac{\partial(\mathcal{I}u_h)}{\partial \mathbf{n}_E} \Big) \, v \, ds$$

$$= \sum_{T\in\mathcal{T}} \int_T R(v - v_T) \, dx - \sum_{E\in\mathcal{E}_0\cup\mathcal{E}_H} \int_E \Big[\!\Big[\frac{\partial(\mathcal{I}u_h)}{\partial \mathbf{n}_E} \Big]\!\Big] (v - v_E) \, ds + \sum_{E\in\mathcal{E}_N} \int_E \frac{\partial e}{\partial \mathbf{n}_E} (v - v_E) \, ds,$$

where we have applied the orthogonalities (4.7), (4.9), and (4.10) for the integral means $v_T = |T|^{-1} \int_T v \, dx$ and $v_E := h_E^{-1} \int_E v \, ds$, respectively. We now apply the Cauchy inequality combined with a Poincaré inequality $\|v - v_T\|_{L^2(T)} \lesssim h_T \|\nabla v\|_{L^2(T)}$ for the first sum and a trace inequality $\|v - v_E\|_{L^2(E)} \lesssim h_E^{1/2} \|\nabla v\|_{L^2(T_E)}$ for the remaining sums, where $T_E \in \mathcal{T}$ is

an arbitrary element with $E \in \mathcal{E}_{T_E}$. This leads to

$$\begin{aligned}\int_\Omega \nabla_{\mathcal{T}} e \cdot \nabla v \, dx &\lesssim \Big(\sum_{T\in\mathcal{T}} h_T^2 \|R\|_{L^2(T)}^2 \Big)^{1/2} \Big(\sum_{T\in\mathcal{T}} \|\nabla v\|_{L^2(T)}^2 \Big)^{1/2} \\ &\quad + \Big(\sum_{E\in\mathcal{E}_0\cup\mathcal{E}_H} h_E \Big\| \Big[\!\Big[\frac{\partial(\mathcal{I}u_h)}{\partial \mathbf{n}_E} \Big]\!\Big] \Big\|_{L^2(E)}^2 \Big)^{1/2} \Big(\sum_{E\in\mathcal{E}_0\cup\mathcal{E}_H} \|\nabla v\|_{L^2(T_E)}^2 \Big)^{1/2} \\ &\quad + \Big(\sum_{E\in\mathcal{E}_N} h_E \Big\| \frac{\partial e}{\partial \mathbf{n}_E} \Big\|_{L^2(E)}^2 \Big)^{1/2} \Big(\sum_{E\in\mathcal{E}_N} \|\nabla v\|_{L^2(T_E)}^2 \Big)^{1/2} \\ &\lesssim \Big[\Big(\sum_{T\in\mathcal{T}} h_T^2 \|R\|_{L^2(T)}^2 \Big)^{1/2} + \Big(\sum_{E\in\mathcal{E}_E} h_E^* \Big\| \Big[\!\Big[\frac{\partial(\mathcal{I}u_h)}{\partial \mathbf{n}_E} \Big]\!\Big] \Big\|_{L^2(E)}^2 \Big)^{1/2} \\ &\quad + \Big(\sum_{E\in\mathcal{E}_N} h_E \Big\| \frac{\partial e}{\partial \mathbf{n}_E} \Big\|_{L^2(E)}^2 \Big)^{1/2} \Big] \|\nabla v\|_{L^2(\Omega)}. \end{aligned} \tag{5.8}$$

For the second integral in (5.7), we proceed in the same manner: Elementwise integration by parts yields

$$\int_\Omega \nabla_{\mathcal{T}} e \cdot \operatorname{curl} w \, dx = -\sum_{T\in\mathcal{T}} \int_{\partial T} \frac{\partial e}{\partial \mathbf{t}_T} w \, ds = -\sum_{T\in\mathcal{T}} \sum_{E\in\mathcal{E}_T\setminus\mathcal{E}_N} \sigma_{T,E} \int_E \frac{\partial e}{\partial \mathbf{t}_E} w \, ds,$$

since $w|_{\Gamma_N} = 0$. Treating the interior edges as before, we obtain

$$\sum_{T\in\mathcal{T}} \sum_{E\in\mathcal{E}_T} \sigma_{T,E} \int_E \frac{\partial e}{\partial \mathbf{t}_E} w \, ds = \sum_{E\in\mathcal{E}_E} \int_E \Big[\!\Big[\frac{\partial(\mathcal{I}u_h)}{\partial \mathbf{t}_E} \Big]\!\Big] w \, ds + \sum_{E\in\mathcal{E}_D} \int_E \frac{\partial e}{\partial \mathbf{t}_E} w \, ds,$$

where we have used that, for an interior edge E, the tangential jump of an H^1-function vanishes, i.e. $[\![\partial u/\partial \mathbf{t}_E]\!]_E = 0$. With the orthogonalities (4.11) and (4.8), we prove

$$\int_\Omega \nabla_{\mathcal{T}} e \cdot \operatorname{curl} w \, dx = -\sum_{E\in\mathcal{E}_E} \int_E \Big[\!\Big[\frac{\partial(\mathcal{I}u_h)}{\partial \mathbf{t}_E} \Big]\!\Big] (w - w_E) \, ds - \sum_{E\in\mathcal{E}_D} \int_E \frac{\partial e}{\partial \mathbf{t}_E} (w - w_E) \, ds$$

for the integral mean $w_E := h_E^{-1} \int_E w \, ds$. As before, the application of the Cauchy inequality and the trace inequality yield

$$\int_\Omega \nabla_{\mathcal{T}} e \cdot \operatorname{curl} w \, dx \lesssim \Big[\sum_{E\in\mathcal{E}_E} h_E^* \Big\| \Big[\!\Big[\frac{\partial(\mathcal{I}u_h)}{\partial \mathbf{t}_E} \Big]\!\Big] \Big\|_{L^2(E)}^2 + \sum_{E\in\mathcal{E}_D} h_E \Big\| \frac{\partial e}{\partial \mathbf{t}_E} \Big\|_{L^2(E)}^2 \Big]^{1/2} \|\nabla w\|_{L^2(\Omega)}. \tag{5.9}$$

If we finally combine (5.7)–(5.9), we prove

$$\begin{aligned}\|\nabla_{\mathcal{T}} e\|_{L^2(\Omega)} \lesssim \Big[&\sum_{T\in\mathcal{T}} h_T^2 \|R\|_{L^2(T)}^2 + \sum_{E\in\mathcal{E}_E} h_E^* \|[\![\nabla \mathcal{I}u_h]\!]\|_{L^2(E)}^2 \\ &+ \sum_{E\in\mathcal{E}_N} h_E \Big\| \frac{\partial e}{\partial \mathbf{n}_E} \Big\|_{L^2(E)}^2 + \sum_{E\in\mathcal{E}_D} h_E \Big\| \frac{\partial e}{\partial \mathbf{t}_E} \Big\|_{L^2(E)}^2 \Big]^{1/2}, \end{aligned}$$

where we have used that $\{\mathbf{t}_E, \mathbf{n}_E\}$ is an orthonormal basis of $\mathbb{R}^2$ and that $\|\nabla v\|_{L^2} \le \|\nabla_{\mathcal{T}} e\|_{L^2}$ as well as $\|\nabla w\|_{L^2} = \|\operatorname{curl} w\|_{L^2} \le \|\nabla_{\mathcal{T}} e\|_{L^2}$. This and $R = f - f_{\mathcal{T}}$ conclude the proof. □

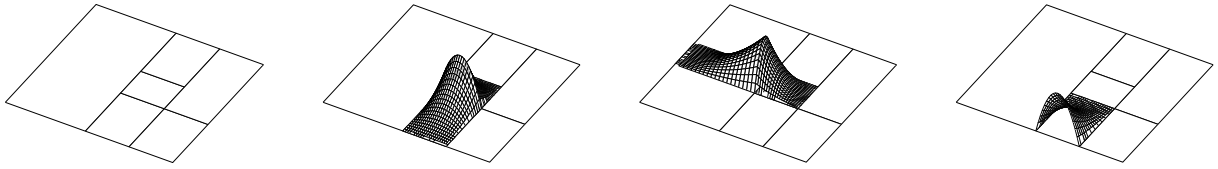

(a) Almost regular triangulation.

(b) Bubble function b_E on $E \in \mathcal{E}_0$.

(c) Bubble function b_E on $E \in \mathcal{E}_E \backslash \mathcal{E}_0$.

(d) Bubble function b_E on a boundary edge.

FIGURE 5.1. *The different types of the edge-bubble functions on an almost regular triangulation.*

5.4. Bubble Functions and Edge Lifting Operator. The elementary edge patch is defined in a way that it belongs to a locally regular triangulation. Therefore, for $E \in \mathcal{E}^*$, we may adopt the notation of the edge-bubble functions and the edge lifting operator from the literature [3, 15].

Lemma 5.4. *For each edge $E \in \mathcal{E}_E \cup \mathcal{E}_D \cup \mathcal{E}_N$, there is a $\widetilde{\omega}_E^*$-piecewise polynomial bubble function $b_E \in H^1(\omega_E^*)$ with $0 \le b_E \le 1$ such that, for all $w \in \mathcal{P}^p(E)$, there holds*

$$c_2 \|w\|_{L^2(E)} \le \|w b_E\|_{L^2(E)} \le \|w\|_{L^2(E)}. \tag{5.10}$$

The constant $c_2 > 0$ depends only on the shape of the elements of $\mathcal{T}$ and the polynomial degree p. Moreover, for $E \in \mathcal{E}^*$, the bubble function satisfies $b_E \in H_0^1(\omega_E^*)$, whereas for a boundary edge $E \in \mathcal{E}_D \cup \mathcal{E}_N$, there holds $b_E|_{\partial\omega_E^* \backslash E} = 0$. □

Lemma 5.5. *For each edge $E \in \mathcal{E}_E \cup \mathcal{E}_D \cup \mathcal{E}_N$, there is a lifting operator $F_{\mathrm{ext}} : \mathcal{P}^p(E) \to H^1(\omega_E^*)$ such that $F_{\mathrm{ext}}(w)|_E = w$, for $w \in \mathcal{P}^p(E)$, as well as*

$$c_3 h_E^{1/2} \|w\|_{L^2(E)} \le \|F_{\mathrm{ext}}(w) b_E\|_{L^2(\omega_E^*)} \le c_4 h_E^{1/2} \|w\|_{L^2(E)} \tag{5.11}$$

and

$$\|\nabla(F_{\mathrm{ext}}(w) b_E)\|_{L^2(\omega_E^*)} \le c_5 h_E^{-1/2} \|w\|_{L^2(E)}. \tag{5.12}$$

The constants $c_3, c_4, c_5 > 0$ depend only on the shape of the elements in $\mathcal{T}$ and the polynomial degree p. Here, b_E denotes the bubble function from Lemma 5.4. □

5.5. Local Efficiency of Error Estimator. To prove efficiency of the proposed error estimator, we need to control the constant $c_6 > 0$ in the estimate $h_E \le h_E^* \le c_6 h_E$ uniformly for all $E \in \mathcal{E}^*$.

Theorem 5.6. *There is a constant $c_7 > 0$ which depends only on c_6 and the shape of the elements in $\mathcal{T}$ but neither on the size nor the number of elements such that*

$$\eta_T^2 \le c_7 \big(\|\nabla_{\mathcal{T}}(u - \mathcal{I}u_h)\|_{L^2(\omega_T)}^2 + h_T^2 \|f - f_{\mathcal{T}}\|_{L^2(\omega_T)}^2 \big), \quad \text{for all } T \in \mathcal{T}. \tag{5.13}$$

We split the proof into 4 claims which dominate the different edge contributions of η_T^2 separately. Throughout the proofs, we adopt the foregoing notations for $e = u - \mathcal{I}u_h$, $R = f + \Delta_{\mathcal{T}}(\mathcal{I}u_h)$ and $\lesssim$.

Claim 1. *There holds* $h_E \Big\| \Big[\!\Big[\dfrac{\partial(\mathcal{I}u_h)}{\partial \mathbf{n}_E} \Big]\!\Big] \Big\|_{L^2(E)}^2 \lesssim \|\nabla_{\mathcal{T}} e\|_{L^2(\omega_E^*)}^2 + h_E^2 \|R\|_{L^2(\omega_E^*)}^2$ *for each $E \in \mathcal{E}_E$.*

Proof. We first stress that $u \in H^1(\Omega)$ implies $\Big[\!\Big[\dfrac{\partial(\mathcal{I}u_h)}{\partial \mathbf{n}_E}\Big]\!\Big]_E = -\Big[\!\Big[\dfrac{\partial e}{\partial \mathbf{n}_E}\Big]\!\Big]_E$. With $b_E \in H^1_0(\omega_E^*)$ the corresponding edge-bubble function, we may define

$$v := F_{\rm ext}\Big(\Big[\!\Big[\frac{\partial(\mathcal{I}u_h)}{\partial \mathbf{n}_E}\Big]\!\Big]_E\Big) b_E \in H^1_0(\omega_E^*).$$

Note that

$$\Big\|\Big[\!\Big[\frac{\partial(\mathcal{I}u_h)}{\partial \mathbf{n}_E}\Big]\!\Big]\Big\|^2_{L^2(E)} \lesssim \int_E \Big[\!\Big[\frac{\partial(\mathcal{I}u_h)}{\partial \mathbf{n}_E}\Big]\!\Big]^2 b_E\,ds = \int_E \Big[\!\Big[\frac{\partial(\mathcal{I}u_h)}{\partial \mathbf{n}_E}\Big]\!\Big]_E v\,ds.$$

We rewrite the right-hand side and use integration by parts to prove

$$\int_E \Big[\!\Big[\frac{\partial(\mathcal{I}u_h)}{\partial \mathbf{n}_E}\Big]\!\Big]_E v\,dx = -\sum_{T\in\widetilde{\omega}_E^*}\int_{\partial T}\frac{\partial e}{\partial \mathbf{n}_T}\,v\,dy = -\sum_{T\in\widetilde{\omega}_E^*}\Big(\int_T \nabla e\cdot\nabla v\,dx - \int_T Rv\,dx\Big).$$

With the help of (5.11)–(5.12), the Cauchy inequality proves

$$\Big\|\Big[\!\Big[\frac{\partial(\mathcal{I}u_h)}{\partial \mathbf{n}_E}\Big]\!\Big]\Big\|^2_{L^2(E)} \lesssim \big(h_E^{-1}\|\nabla_{\mathcal{T}} e\|^2_{L^2(\omega_E^*)} + h_E\|R\|^2_{L^2(\omega_E^*)}\big)^{1/2}\Big\|\Big[\!\Big[\frac{\partial(\mathcal{I}u_h)}{\partial \mathbf{n}_E}\Big]\!\Big]\Big\|_{L^2(E)}. \qquad \square$$

Claim 2. *There holds* $h_E\Big\|\Big[\!\Big[\dfrac{\partial(\mathcal{I}u_h)}{\partial \mathbf{t}_E}\Big]\!\Big]\Big\|^2_{L^2(E)} \lesssim \|\nabla_{\mathcal{T}} e\|^2_{L^2(\omega_E^*)}$ *for each* $E \in \mathcal{E}_E$.

Proof. With $b_E \in H^1_0(\omega_E^*)$ the corresponding edge-bubble function, we observe

$$\Big\|\Big[\!\Big[\frac{\partial(\mathcal{I}u_h)}{\partial \mathbf{t}_E}\Big]\!\Big]\Big\|^2_{L^2(E)} \lesssim \int_E \Big[\!\Big[\frac{\partial(\mathcal{I}u_h)}{\partial \mathbf{t}_E}\Big]\!\Big] v\,ds \quad \text{with} \quad v := F_{\rm ext}\Big(\Big[\!\Big[\frac{\partial(\mathcal{I}u_h)}{\partial \mathbf{t}_E}\Big]\!\Big]_E\Big) b_E \in H^1_0(\omega_E^*).$$

As before, we rewrite the right-hand side and use integration by parts to prove

$$\int_E \Big[\!\Big[\frac{\partial(\mathcal{I}u_h)}{\partial \mathbf{t}_E}\Big]\!\Big] v\,ds = \sum_{T\in\widetilde{\omega}_E^*}\int_{\partial T}\frac{\partial(\mathcal{I}u_h)}{\partial \mathbf{t}_T}\,v\,dx = -\sum_{T\in\widetilde{\omega}_E^*}\int_T \nabla(\mathcal{I}u_h)\cdot\operatorname{curl} v\,dx.$$

Together with $\int_{\omega_E^*}\nabla u\cdot\operatorname{curl} v\,dx = 0$ and (5.12), we obtain

$$\begin{aligned}\Big\|\Big[\!\Big[\frac{\partial(\mathcal{I}u_h)}{\partial \mathbf{t}_E}\Big]\!\Big]\Big\|^2_{L^2(E)} &\lesssim \int_{\omega_E^*}\nabla_{\mathcal{T}} e\cdot\operatorname{curl} v\,dx \le \|\nabla_{\mathcal{T}} e\|_{L^2(\omega_E^*)}\|\nabla v\|_{L^2(\omega_E^*)}\\ &\lesssim h_E^{-1/2}\|\nabla_{\mathcal{T}} e\|_{L^2(\omega_E^*)}\Big\|\Big[\!\Big[\frac{\partial(\mathcal{I}u_h)}{\partial \mathbf{t}_E}\Big]\!\Big]\Big\|_{L^2(E)},\end{aligned}$$

where we used $\|\operatorname{curl} v\|_{L^2} = \|\nabla v\|_{L^2}$. $\square$

Claim 3. *For* $E \in \mathcal{E}_D$, *there holds* $h_E\Big\|\dfrac{\partial e}{\partial \mathbf{t}_E}\Big\|^2_{L^2(E)} \lesssim \|\nabla e\|^2_{L^2(T)}$.

Proof. For $E \in \mathcal{E}_D$, there is a unique element $\omega_E = T \in \mathcal{T}$ with $E \in \mathcal{E}_T$. The corresponding edge-bubble function $b_E \in H^1(T)$ satisfies $b_E|_{\partial T\setminus E} = 0$. We consider

$$v := F_{\rm ext}\Big(\frac{\partial e}{\partial \mathbf{t}_E}\Big) b_E \in H^1(T)$$

and note that $v|_{\partial T\setminus E} = 0$ as well as $\mathbf{t}_T|_E = \mathbf{t}_E$. Therefore,

$$\Big\|\frac{\partial e}{\partial \mathbf{t}_E}\Big\|^2_{L^2(E)} \lesssim \int_E \frac{\partial e}{\partial \mathbf{t}_E}\,v\,ds = \int_{\partial T}\frac{\partial e}{\partial \mathbf{t}_T}\,v\,ds = -\int_T \nabla e\cdot\operatorname{curl} v\,dx$$

The application of the Cauchy inequality together with (5.12) yields

$$-\int_T \nabla e \cdot \operatorname{curl} v \, dx \le h_E^{-1/2} \|\nabla e\|_{L^2(T)} \Big\| \frac{\partial e}{\partial \mathbf{t}_E} \Big\|_{L^2(E)},$$

which concludes the proof. □

Claim 4. *For $E \in \mathcal{E}_N$, holds $h_E \Big\| \dfrac{\partial e}{\partial \mathbf{n}_E} \Big\|_{L^2(E)}^2 \lesssim \|\nabla e\|_{L^2(T)}^2 + h_E^2 \|R\|_{L^2(T)}^2$.*

Proof. As in Claim 3, let $T \in \mathcal{T}$ be the unique element with $\omega_E = T$ for a fixed edge $E \in \mathcal{E}_N$ and let $b_E \in H^1(T)$ be the associated edge bubble function. With

$$v := F_{\text{ext}}\Big(\frac{\partial e}{\partial \mathbf{n}_E}\Big) b_E \in H^1(T)$$

and integration by parts, there holds

$$\Big\| \frac{\partial e}{\partial \mathbf{n}_E} \Big\|_{L^2(E)}^2 \lesssim \int_{\partial T} \frac{\partial e}{\partial \mathbf{n}_T} \, v \, ds = \int_T \nabla e \cdot \nabla v \, dx - \int_T R v \, dx.$$

The proof now follows as in Claim 1. □

Proof of Theorem 5.6. According to Claim 1 and 2, there holds

$$\begin{aligned} \sum_{E \in \mathcal{E}_T \cap \mathcal{E}_E} h_E^* \|[\![\nabla_{\mathcal{T}} (\mathcal{I} u_h)]\!]\|_{L^2(E)}^2 &\lesssim \sum_{E \in \mathcal{E}_T \cap \mathcal{E}_E} \big(\|\nabla_{\mathcal{T}} e\|_{L^2(\omega_E^*)}^2 + h_E^2 \|R\|_{L^2(\omega_E^*)}^2 \big) \\ &\lesssim \|\nabla_{\mathcal{T}} e\|_{L^2(\omega_T)}^2 + h_E^2 \|R\|_{L^2(\omega_T)}^2. \end{aligned}$$

With Claim 3, there holds

$$\sum_{E \in \mathcal{E}_T \cap \mathcal{E}_D} h_E \Big\| \frac{\partial e}{\partial \mathbf{t}_E} \Big\|_{L^2(E)}^2 \lesssim \sum_{E \in \mathcal{E}_T \cap \mathcal{E}_D} \|\nabla e\|_{L^2(T)}^2 \le 4 \|\nabla e\|_{L^2(T)}^2.$$

With Claim 4, there holds

$$\begin{aligned} \sum_{E \in \mathcal{E}_T \cap \mathcal{E}_N} h_E \Big\| \frac{\partial e}{\partial \mathbf{n}_E} \Big\|_{L^2(E)}^2 &\lesssim \sum_{E \in \mathcal{E}_T \cap \mathcal{E}_N} \big(\|\nabla e\|_{L^2(T)}^2 + h_E^2 \|R\|_{L^2(T)}^2 \big) \\ &\le 4 \big(\|\nabla e\|_{L^2(T)}^2 + h_E^2 \|R\|_{L^2(T)}^2 \big) \end{aligned}$$

Finally, this and $R = f - f_{\mathcal{T}}$ prove (5.13). □

6. Numerical Experiments

In this section, we study the accuracy of the derived a posteriori error estimate from Section 5 as well as the performance of an adaptive mesh-refining algorithm which is steered by the local refinement indicators η_T from (5.1). All computations are done in MATLAB. Throughout, we run the following standard algorithm, where we use $\theta = 0$ for uniform and $\theta = 0.5$ for adaptive mesh-refinement, respectively.

Algorithm 6.1. *Given an initial mesh $\mathcal{T}^{(0)}$, $k = 0$, and $0 \le \theta \le 1$, do the following:*

1. *Compute the discrete solution $u_h \in \mathcal{P}^0(\mathcal{T}^{(k)})$ for the current mesh $\mathcal{T}^{(k)} = \{T_1, \dots, T_N\}$.*
2. *Compute the Morley interpolant $\mathcal{I} u_h$.*
3. *Compute the refinement indicators η_{T_j} for all elements $T_j \in \mathcal{T}^{(k)}$.*
4. *Mark element T_j provided that η_{T_j} satisfies $\eta_{T_j} \ge \theta \max\{\eta_{T_1}, \dots, \eta_{T_N}\}$.*

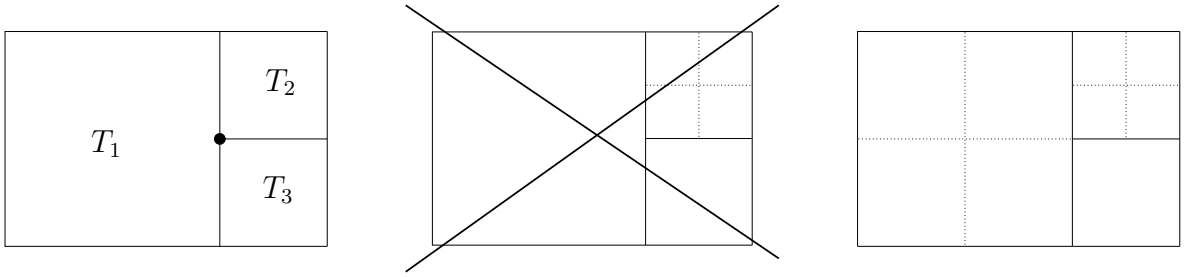

(a) *original mesh* (b) *not allowed* (c) *allowed*

FIGURE 6.1. *To bound the constant c_6 which enters the efficiency estimate of Theorem 5.6, we only allow one hanging node per edge: If in configuration* (a) *the element T_2 is marked for refinement, we mark element T_1 for refinement as well. This leads to configuration* (c) *instead of* (b) *after refinement.*

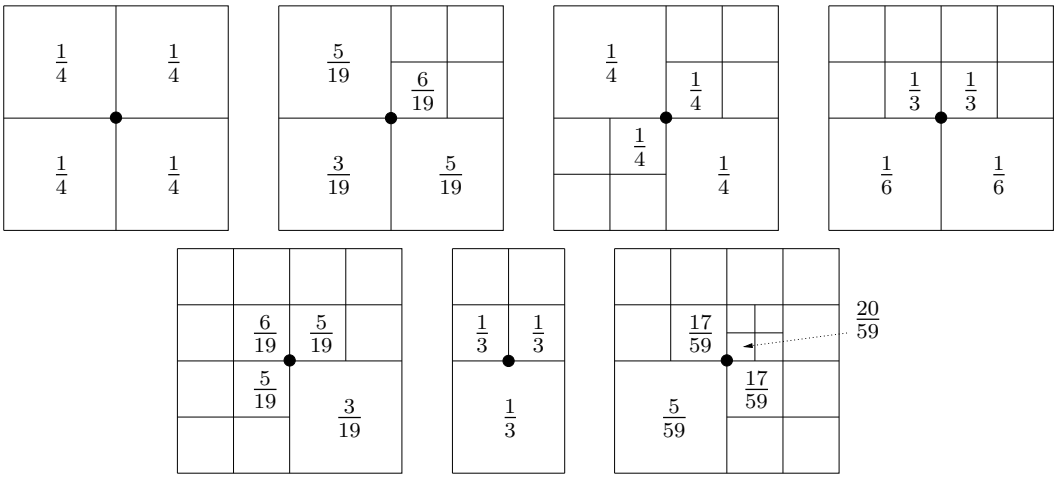

FIGURE 6.2. *A priori computed weights ψ_T for the special mesh of squares with at most one hanging node per edge.*

(5) *Refine all marked elements $T_j \in \mathcal{T}^{(k)}$ and generate a new mesh $\mathcal{T}^{(k+1)}$.*
(6) *Update $k \mapsto k+1$ and go to* (1). □

In all experiments, the initial mesh $\mathcal{T}^{(0)}$ is a uniform and regular triangulation, where all of the elements are either triangles or squares. In case of triangular elements, we use a red-green-blue strategy to obtain $\mathcal{T}^{(k+1)}$ from $\mathcal{T}^{(k)}$, i.e. marked elements are uniformly refined and the obtained mesh is regularized by a green-blue closure [15]. In case of square elements, a marked element is uniformly refined, and we allow hanging nodes. However, we do some additional marking to ensure the following assumption.

Assumption 1. *For all almost regular meshes consisting of squares, there is at most one step of refinement between two neighbouring cells, cf. Figure 6.1.* □

Note that under this assumption, there are only 7 possible geometrical configurations for triangulations with square elements. This allows the a priori computation of the weights $\psi_T(a)$ in (3.7) and (4.3) which is shown in Figure 6.2.

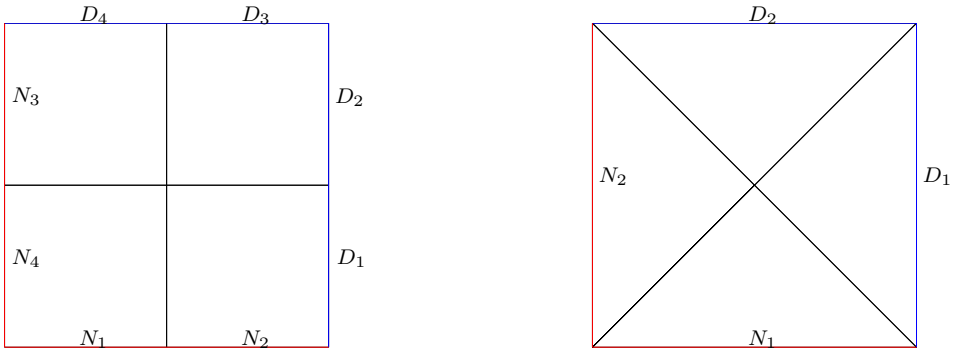

FIGURE 6.3. *Domain $\Omega = (0,1)^2$ as well as Dirichlet and Neumann boundary conditions in Example 6.1. The initial mesh $\mathcal{T}^{(0)}$ consists of four squares (left) and four triangles (right), respectively.*

Throughout, we compute and compare the following numerical quantities for uniform and adaptive mesh-refinement: First, the Morley error

$$E_{\mathcal{I}} := \|\nabla_{\mathcal{T}}(u - \mathcal{I}u_h)\|_{L^2(\Omega)}, \tag{6.1}$$

where $\mathcal{I}$ denotes the Morley interpolant. Second, the corresponding residual-based error estimator

$$\eta := \Big(\sum_{T\in\mathcal{T}} \eta_T^2\Big)^{1/2}, \tag{6.2}$$

where η_T are the refinement indicators of (5.1). Finally, the discretization error in the discrete H^1-norm

$$E_h := \|u - u_h\|_{1,h} := \big(\|u - u_h\|_{L^2(\Omega)}^2 + |u_{\mathcal{T}} - u_h|_{1,h}^2\big)^{1/2}, \tag{6.3}$$

where $u_{\mathcal{T}} \in \mathcal{P}^0(\mathcal{T})$ is the $\mathcal{T}$-piecewise integral mean of u, i.e. $u_{\mathcal{T}}|_T = |T|^{-1}\int_T u\,dx$, and where the discrete H^1-seminorm is defined by

$$|v_h|_{1,h} = \Big(\sum_{E\in\mathcal{E}_E\cup\mathcal{E}_D} \Big|\frac{v_{T_E} - v_{T_W}}{d_E}\Big|^2 h_E d_E\Big)^{1/2}$$

for any $\mathcal{T}$-piecewise constant function $v_h \in \mathcal{P}^0(\mathcal{T})$. According to [9], the diamond path method satisfies $E_h = \mathcal{O}(h)$ with $h = \max_{T\in\mathcal{T}} h_T$ provided that $u \in H^2(\Omega)$. We stress that this, however, is only proven for locally refined Cartesian meshes, i.e. meshes consisting of rectangular elements with at most one hanging node per edge. In case of triangular meshes, the proof still seems to be open.

6.1. Example with Smooth Solution. We consider the Laplace problem (1.1) on the unit square $\Omega = (0,1)^2$ with prescribed exact solution

$$u(x,y) = \sinh(\pi x)\cos(\pi y) \quad \text{for } (x,y) \in \Omega. \tag{6.4}$$

Note that u is smooth and satisfies $f := \Delta u = 0$ so that the data oscillation term $\|h(f - f_{\mathcal{T}})\|_{L^2(\Omega)}$ of the error estimator η vanishes. We consider mixed boundary conditions, where

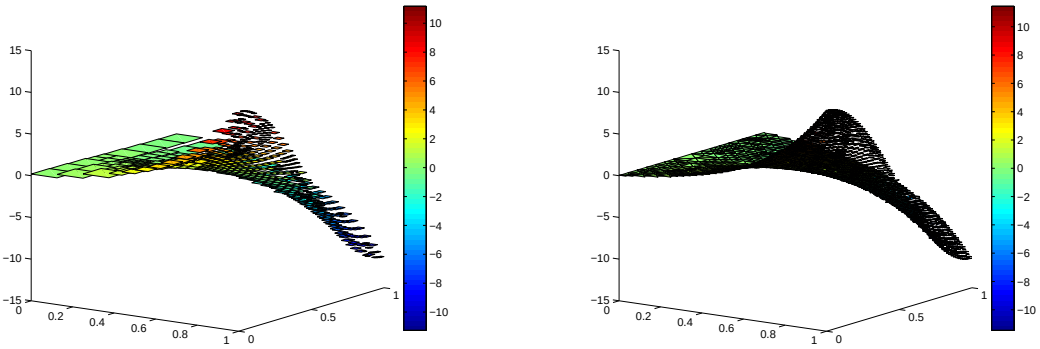

FIGURE 6.4. *$\mathcal{T}$-piecewise constant solutions u_h in Example 6.1 with respect to adaptively generated meshes $\mathcal{T}^{(10)}$ consisting of $\#\mathcal{T}^{(10)} = 706$ squares (left) and $\#\mathcal{T}^{(10)} = 3967$ triangles (right), respectively.*

the Dirichlet and Neumann data on

$$\Gamma_D = \{1\} \times [0,1] \cup [0,1] \times \{1\} \quad \text{and} \quad \Gamma_N = (0,1) \times \{0\} \cup \{0\} \times (0,1) \tag{6.5}$$

are computed from the given exact solution. The initial mesh $\mathcal{T}^{(0)}$ consists of either 4 squares or 4 triangles, cf. Figure 6.3.

Figure 6.5 shows the curves of the errors $E_{\mathcal{I}} = \|\nabla_{\mathcal{T}}(u - \mathcal{I}u_h)\|_{L^2(\Omega)}$ and $E_h = \|u - u_h\|_{1,h}$ as well as the curve of the error estimator η with respect to uniform and adaptive mesh-refinement. We plot the experimental results over the number of elements, where both axes are scaled logarithmically. Therefore, a straight line g with slope $-\alpha$ corresponds to a dependence $g = \mathcal{O}(N^{-\alpha})$, where $N = \#\mathcal{T}$ denotes the number of elements. Note that, for uniform mesh-refinement the order $\mathcal{O}(N^{-\alpha})$ with respect to N corresponds to $\mathcal{O}(h^{2\alpha})$ with respect to the maximal mesh-size $h := \max_{T \in \mathcal{T}} h_T$.

Because of $u \in H^2(\Omega)$, theory predicts the optimal order of convergence $E_h = \mathcal{O}(N^{-1/2})$ in case of uniform mesh-refinement and square elements. This is, in fact, observed. Moreover, in case of square elements, the curves of E_h for uniform and adaptive mesh-refinement almost coincide. However, the adaptive algorithm does not lead to uniformly refined meshes. Instead, the adaptive meshes plotted in Figure 6.6 show a certain refinement towards the edge $x = 1$ since the gradient of $u(x, y)$ is increasing with $x \to 1$, cf. Figure 6.4, where we visualize some computed discrete solutions u_h. Although the Dirichlet and Neumann boundary are not chosen symmetrically, the adaptive meshes appear to be almost symmetric with respect to the line $y = 1/2$, which corresponds to the symmetry $|\nabla u(x, 1/2 - y)| = |\nabla u(x, 1/2 + y)|$ of the exact solution.

For triangular elements, we observe the order $\mathcal{O}(N^{-1/2})$ for both uniform and adaptive mesh-refinement. However, the absolute values of E_h are better in case of uniform mesh-refinement. As in case of rectangular elements, we observe a certain refinement of the adaptively generated meshes towards the right edge $x = 1$ in Figure 6.7, and again they are almost symmetric related to the line $y = 1/2$.

For the Morley error $E_{\mathcal{I}}$ and uniform mesh-refinement, we experimentally observe some superconvergence of order 3/4 for both square and triangular elements in Figure 6.5. This superconvergence is destroyed by use of adaptive mesh-refinement, where we only observe a convergence order 1/2. Independently of the mesh-refining strategy and the type of elements,

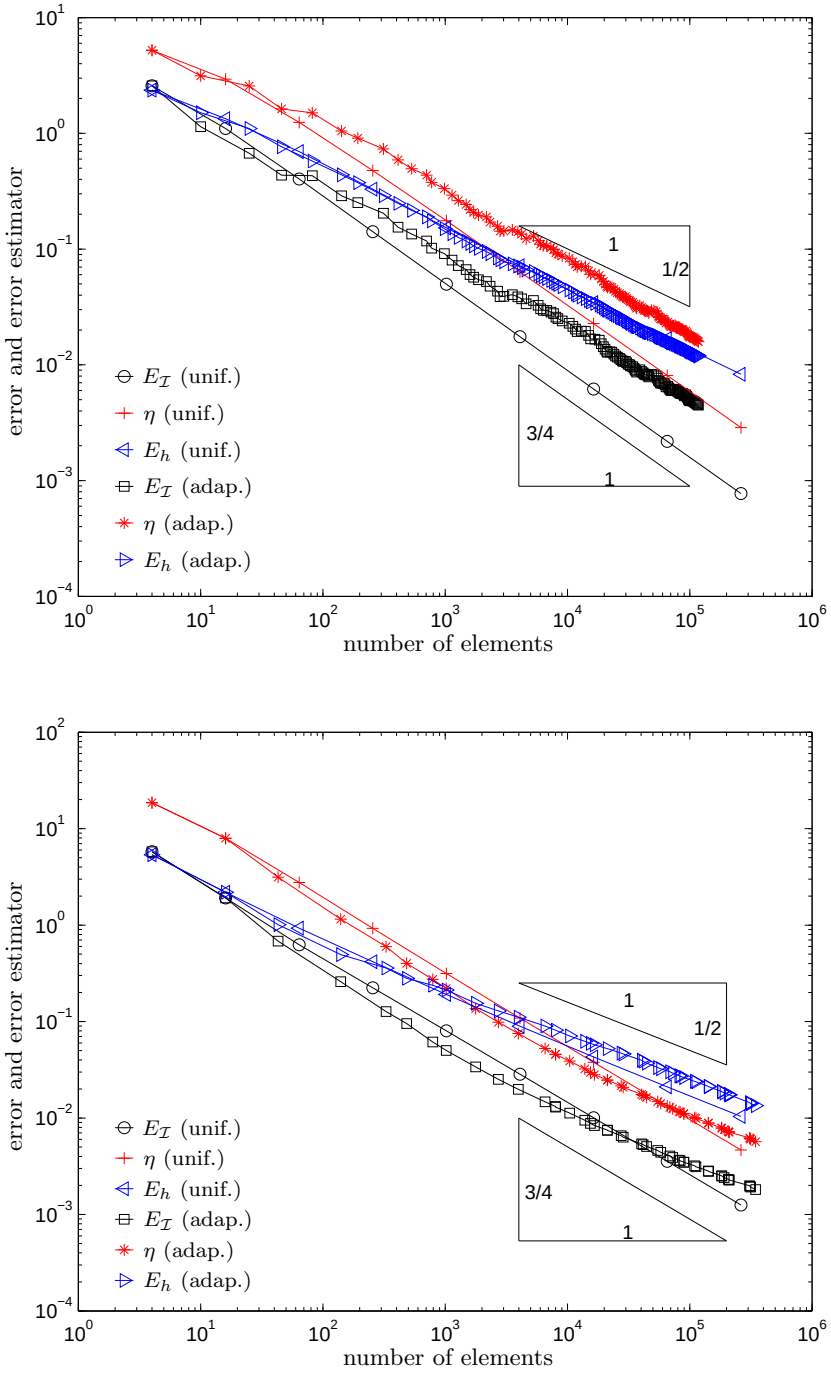

FIGURE 6.5. *Morley error* $E_{\mathcal{I}} = \|\nabla_{\mathcal{T}}(u - \mathcal{I}u_h)\|_{L^2(\Omega)}$ *and corresponding error estimator* η *as well as energy error* $E_h = \|u - u_h\|_{1,h}$ *in Example 6.1 for uniform and adaptive mesh-refinement and triangulations consisting of squares (top) and triangles (bottom), respectively.*

we observe the theoretically predicted reliability and efficiency of the error estimator η: The

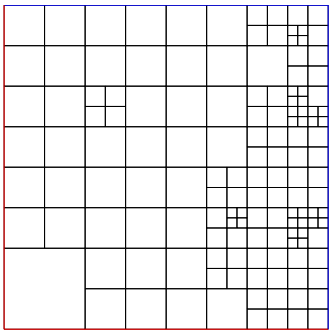

$\#\mathcal{T}^{(5)} = 142$

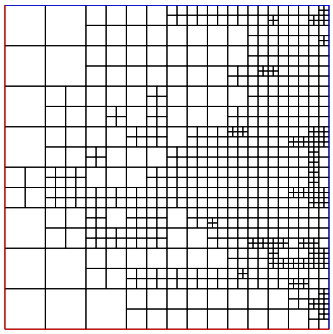

$\#\mathcal{T}^{(10)} = 706$

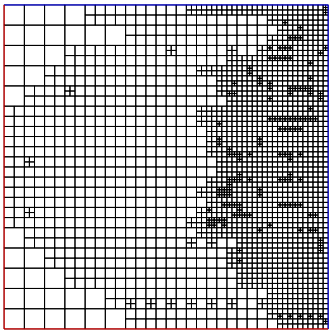

$\#\mathcal{T}^{(20)} = 2329$

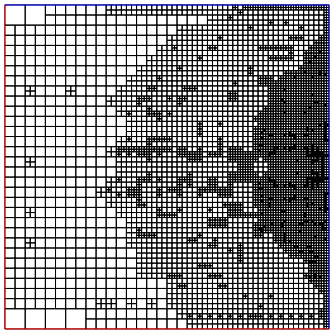

$\#\mathcal{T}^{(30)} = 6034$

FIGURE 6.6. *Adaptively generated meshes* $\mathcal{T}^{(k)}$ *for* $k = 5, 10, 20, 30$ *with square elements in Example 6.1.*

curves of the Morley error $E_{\mathcal{I}}$ and the corresponding error estimator η are parallel up to a certain range.

6.2. Laplace Problem with Generic Singularity. We consider the Laplace problem (1.1) on the L-shaped domain

$$\Omega = (-1,1)^2 \backslash \big([0,1] \times [-1,0]\big) \tag{6.6}$$

as shown in Figure 6.8. The given exact solution is the harmonic function $u(x,y) = \Im\big((x+iy)^{2/3}\big)$ and reads in polar coordinates

$$u(x,y) = r^{2/3} \sin(2\varphi/3) \quad \text{with} \quad (x,y) = r\,(\cos\varphi, \sin\varphi). \tag{6.7}$$

Note that u has a generic singularity at the reentrant corner $(0,0)$, which leads to $u \in H^{1+2/3-\varepsilon}(\Omega)$ for all $\varepsilon > 0$. Therefore, a conforming finite element method with polynomial ansatz space leads to convergence of order $\mathcal{O}(h^{2/3})$ for the finite element error in the H^1-norm, where h denotes the uniform mesh-size. This corresponds to order $\mathcal{O}(N^{-1/3})$ with respect to the number of elements.

For the numerical computation, we prescribe the exact Neumann and Dirichlet data, where

$$\Gamma_D = \Gamma \backslash \Gamma_N \quad \text{and} \quad \Gamma_N := \{0\} \times (-1,0) \cup (0,1) \times \{0\}. \tag{6.8}$$

The initial meshes as well as Γ_D and Γ_N are shown in Figure 6.8. Note that Γ_N includes the reentrant corner, where the normal derivative $\partial u/\partial \mathbf{n}$ is singular.

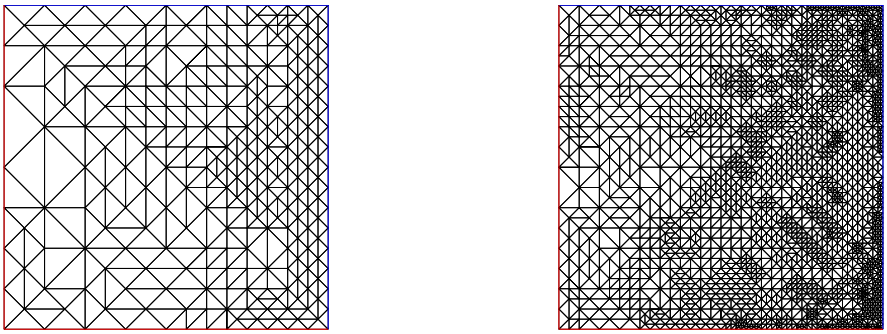

$\#\mathcal{T}^{(5)} = 484$ $\#\mathcal{T}^{(10)} = 3967$

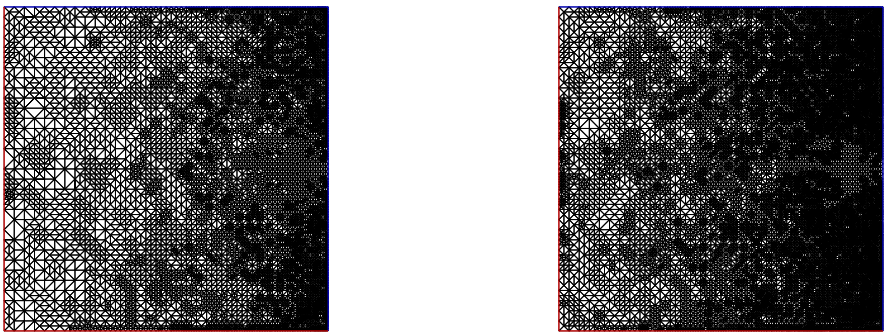

$\#\mathcal{T}^{(15)} = 13867$ $\#\mathcal{T}^{(20)} = 27518$

FIGURE 6.7. *Adaptively generated meshes $\mathcal{T}^{(k)}$ for $k = 5, 10, 15, 20$ with triangular elements in Example 6.1.*

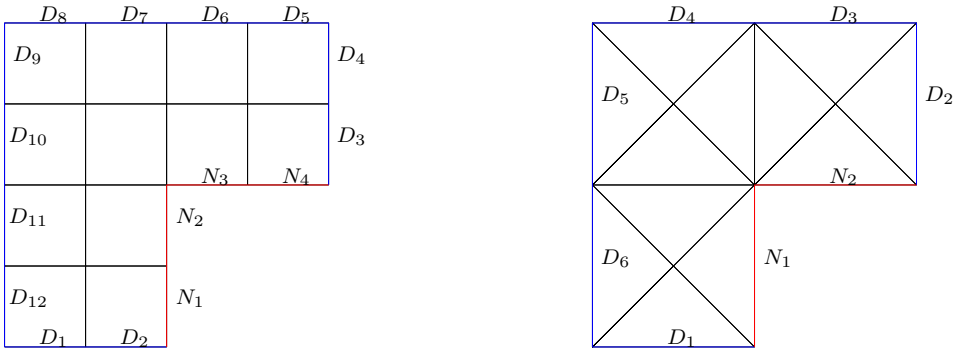

FIGURE 6.8. *L-shaped domain as well as Dirichlet and Neumann boundary conditions in Laplace Problem 6.2. The initial mesh $\mathcal{T}^{(0)}$ consists of twelve squares (left) and twelve triangles (right), respectively.*

Figure 6.9 plots the experimental results for the energy error E_h as well as for the Morley error $E_{\mathcal{I}}$ and the corresponding error estimator η over the number of elements. For uniform mesh-refinement, the energy error E_h converges with a suboptimal order which appears to be slightly better than $\mathcal{O}(N^{-1/3})$ for both square and triangular elements. The proposed adaptive strategy regains the optimal order of convergence $\mathcal{O}(N^{-1/2})$.

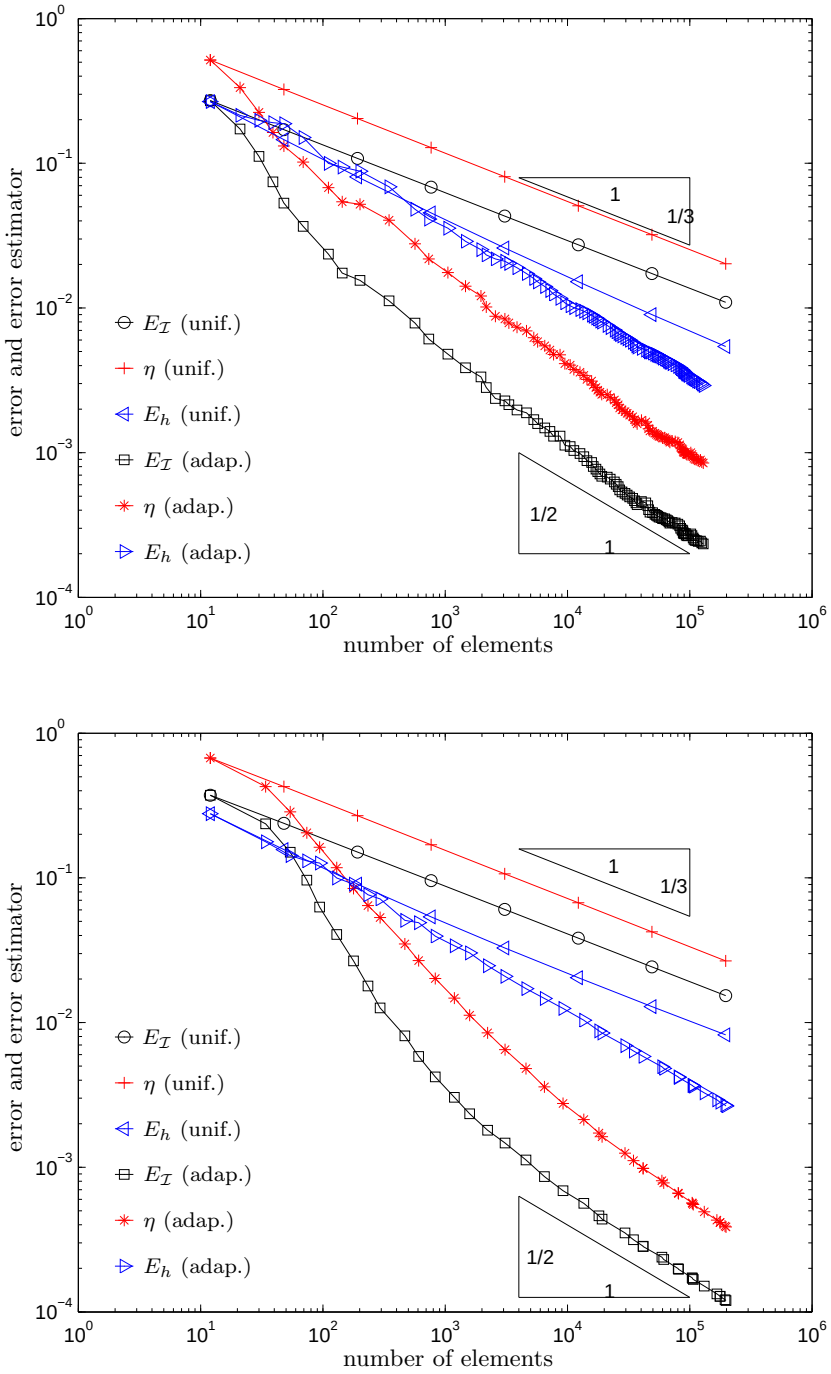

FIGURE 6.9. *Morley error* $E_\mathcal{I} = \|\nabla_\mathcal{T}(u - \mathcal{I}u_h)\|_{L^2(\Omega)}$ *and corresponding error estimator* η *as well as energy error* $E_h = \|u - u_h\|_{1,h}$ *in Laplace Problem 6.2 for uniform and adaptive mesh-refinement and triangulations consisting of squares (top) and triangles (bottom), respectively.*

As can be expected from the finite element method, the Morley error $E_\mathcal{I}$ decreases like $\mathcal{O}(N^{-1/3})$ for uniform mesh-refinement. The adaptive algorithm leads to an improved order of convergence $\mathcal{O}(N^{-1/2})$. For both mesh-refining strategies as well as for square and triangular elements, the error estimator η is observed to be reliable and efficient.

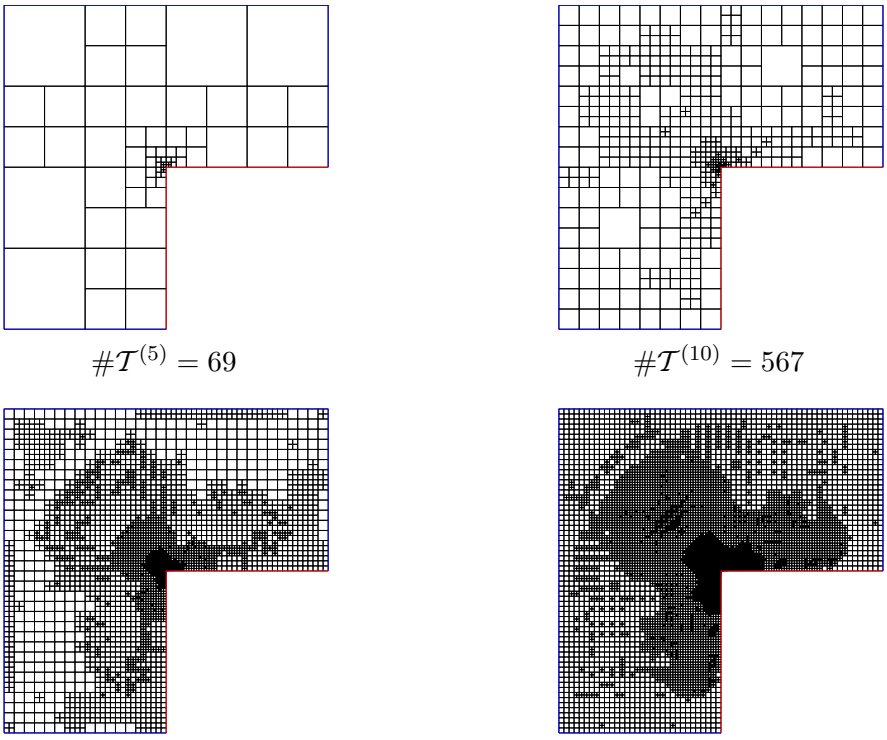

$\#\mathcal{T}^{(5)} = 69$ $\#\mathcal{T}^{(10)} = 567$

$\#\mathcal{T}^{(20)} = 4629$ $\#\mathcal{T}^{(30)} = 12666$

FIGURE 6.10. *Adaptively generated meshes* $\mathcal{T}^{(k)}$ *for* $k = 5, 10, 20, 30$ *with square elements in Laplace Problem 6.2.*

6.3. Laplace Problem with Inhomogeneous Right-Hand Side. Finally, we consider the Laplace problem (1.1) on the L-shaped domain (6.6) from the previous experiment. The exact solution is prescribed by $u(x,y) = \Im\big((x+iy)^{2/3}\big) + \big(x^2+y^2\big)^{3/2}$ and reads in polar coordinates

$$u(x,y) = r^{2/3}\sin(2\varphi/3) + r^3 \quad \text{with} \quad (x,y) = r\,(\cos\varphi, \sin\varphi). \tag{6.9}$$

Note that $f = -\Delta u$ reads $f(x,y) = -9\,(x^2+y^2)^{1/2}$ resp. $f(x,y) = -9\,r$ with respect to polar coordinates. We consider mixed boundary conditions with Γ_D and Γ_N as in the previous experiment. Figure 6.12 shows the numerical results of our computation. Despite a pre-asymptotic phase, where the f has to be resolved, we observe the same behaviour as in Example 6.2.

APPENDIX A. ELEMENTARY PROOF OF TRACE INEQUALITY

In this section, we give a somehow elementary proof of the trace inequality

$$\|v - v_T\|_{L^2(E)} \le c_8 h_E^{1/2} \|\nabla v\|_{L^2(T)} \quad \text{for } v \in H^1(T), \tag{A.1}$$

where $v_T := |T|^{-1}\int_T v\,dx$ is the integral mean of v and T is a triangle or rectangle in $\mathbb{R}^2$ with edge E. We stress that all proofs even work for arbitrary dimension $d \ge 2$ and T a tetrahedron or cuboid, respectively. The analysis is elementary in the sense that we

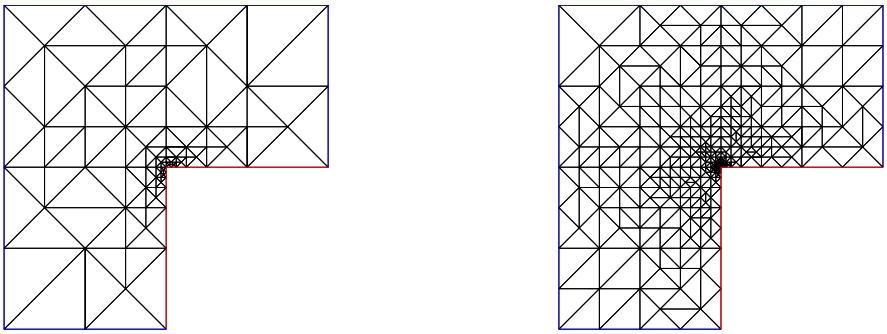

$\#\mathcal{T}^{(5)} = 130$ $\#\mathcal{T}^{(10)} = 608$

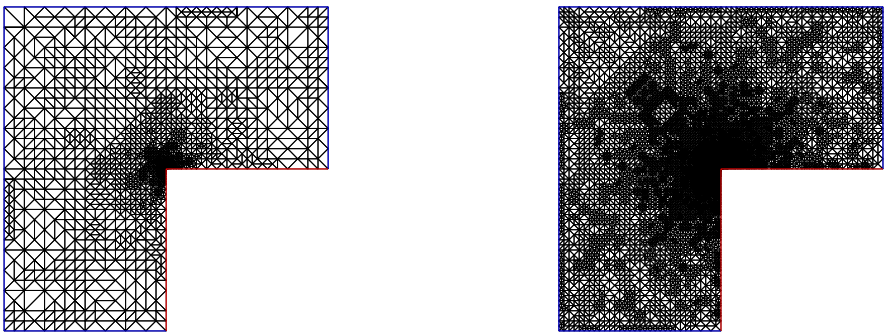

$\#\mathcal{T}^{(15)} = 3090$ $\#\mathcal{T}^{(20)} = 18070$

FIGURE 6.11. *Adaptively generated meshes* $\mathcal{T}^{(k)}$ *for* $k = 5, 10, 15, 20$ *with triangular elements in Laplace Problem 6.2.*

provide trace identities and then only make use of the Poincaré inequality $\|v - v_T\|_{L^2(T)} \leq c_9 h_T \|\nabla v\|_{L^2(T)}$, where $c_9 = 1/\pi$ is known to be the optimal constant [2, 14].

***Remark* A.1.** In the literature, the trace inequality often reads $\|v - v_T\|_{L^2(E)} \leq c_8 \|\nabla v\|_{L^2(\omega_E)}$, cf. [1]. We stress that our version (A.1) does only involve the L^2-norm over T instead over the patch ω_E on the right-hand side.

Theorem A.1. (i) *Let* $T = \operatorname{conv}\{a_1, a_2, a_3\}$ *be a nondegenerate triangle and* $E = \operatorname{conv}\{a_1, a_2\}$. *Then, there holds for* $w \in W^{1,1}(T)$

$$\frac{1}{|T|} \int_T w \, dx = \frac{1}{h_E} \int_E w \, ds - \frac{1}{2|T|} \int_T (x - a_3) \cdot \nabla w(x) \, dx. \tag{A.2}$$

(ii) *Let* $T = \operatorname{conv}\{a_1, a_2, a_3, a_4\}$ *be a nondegenerate rectangle and* $E = \operatorname{conv}\{a_1, a_2\}$. *Then, there holds for* $w \in W^{1,1}(T)$

$$\frac{1}{|T|} \int_T w \, dx = \frac{1}{h_E} \int_E w \, ds - \frac{1}{|T|} \int_T \mathbf{n}_E \cdot (x - a_4) \, \mathbf{n}_E \cdot \nabla w(x) \, dx, \tag{A.3}$$

where $\mathbf{n}_E$ *is the outer normal vector of* T *on* E.

Proof for Triangles [5]. We first consider the reference element $T_{\mathrm{ref}} = \operatorname{conv}\{(0,1), (0,0), (1,0)\}$ with reference edge $E_{\mathrm{ref}} = \{0\} \times [0,1]$. Note that $a_3^{\mathrm{ref}} = (1,0)$ and the outer normal vector of T_{ref} on E_{ref} is $\mathbf{n}_E^{\mathrm{ref}} = (-1,0)$. We consider the function $g(y) = w(y)(y - a_3^{\mathrm{ref}})$. Note that $(y - a_3^{\mathrm{ref}}) \cdot \mathbf{n}_{T_{\mathrm{ref}}}(y) = 1$ for $y \in E_{\mathrm{ref}}$ and $(y - a_3^{\mathrm{ref}}) \cdot \mathbf{n}_{T_{\mathrm{ref}}}(y) = 0$ for $y \in \partial T_{\mathrm{ref}} \backslash E_{\mathrm{ref}}$. The Gauss

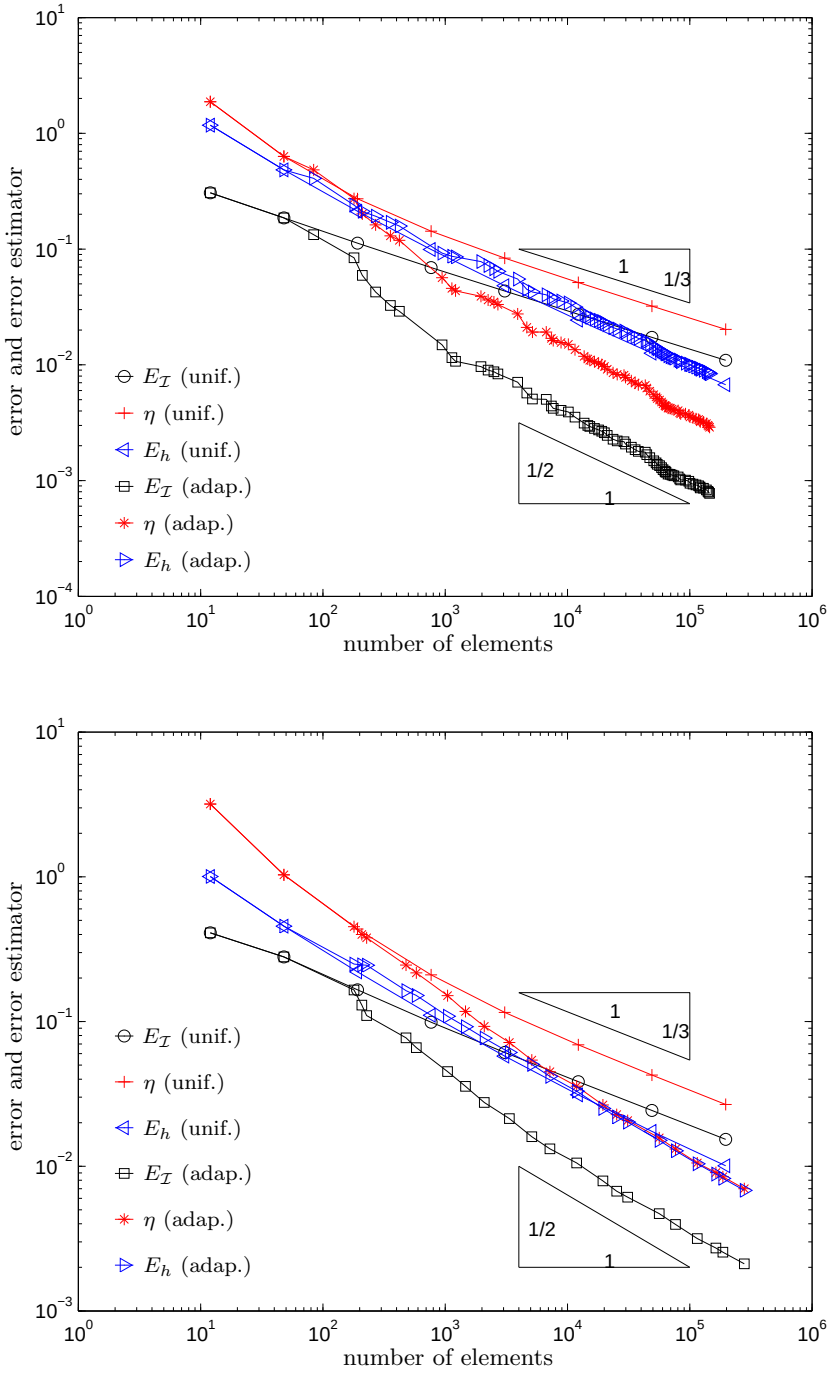

FIGURE 6.12. *Morley error* $E_\mathcal{I} = \|\nabla_\mathcal{T}(u - \mathcal{I}u_h)\|_{L^2(\Omega)}$ *and corresponding error estimator* η *as well as energy error* $E_h = \|u - u_h\|_{1,h}$ *in Laplace Problem 6.3 for uniform and adaptive mesh-refinement and triangulations consisting of squares (top) and triangles (bottom), respectively.*

divergence theorem proves

$$\int_{E_{\mathrm{ref}}} w\,dx = \int_{\partial T_{\mathrm{ref}}} g\cdot\mathbf{n}_{T_{\mathrm{ref}}}\,ds = \int_{T_{\mathrm{ref}}} \operatorname{div} g\,dy = \int_{T_{\mathrm{ref}}} \nabla w(y)\cdot(y-a_3^{\mathrm{ref}})\,dy + 2\int_{T_{\mathrm{ref}}} w\,dy$$

which concludes the proof of the reference case since $|T_{\mathrm{ref}}| = 1/2$. With an affine bijection Φ_T that maps $T_{\mathrm{ref}} \mapsto T$ and $E_{\mathrm{ref}} \mapsto E$, the general proof of (A.2) follows from integral transformations. □

Proof for Rectangles. We consider the reference element $T_{\mathrm{ref}} = [0,1]^2$ with edge $E_{\mathrm{ref}} = \{0\} \times [0,1]$. Note that $a_4^{\mathrm{ref}} = (1,1)$ and the outer normal vector of T_{ref} on E_{ref} is $\mathbf{n}_E^{\mathrm{ref}} = (-1,0)$. To verify (A.3) in this case, we consider the function $g(y) = (y_1 - 1)w(y)$ on T_{ref}. The main theorem of calculus proves

$$w(0,y_2) = g(1,y_2) - g(0,y_2) = \int_0^1 \partial_1 g(y)\,dy_1 = \int_0^1 w(y)\,dy_1 + \int_0^1 (y_1-1)\partial_1 w(y)\,dy_1.$$

Integrating this equality over $[0,1]$, we obtain

$$\int_{E_{\mathrm{ref}}} w\,ds = \int_{T_{\mathrm{ref}}} w\,dy + \int_{T_{\mathrm{ref}}} (y_1-1)\partial_1 w(y)\,dy.$$

Finally, there holds $(y_1-1)\partial_1 w(y) = \mathbf{n}_E^{\mathrm{ref}} \cdot (y - a_4^{\mathrm{ref}})\mathbf{n}_E^{\mathrm{ref}} \cdot \nabla w(y)$, which concludes the proof of the reference case. Again, the proof of the general case follows by affine transformation. □

Corollary A.2. *Suppose that $T \subset \mathbb{R}^2$ is either a nondegenerate triangle or rectangle. Then, there holds* (A.1)*, where $c_8 > 0$ only depends on the shape of T but not on its size.*

Proof. Plugging $w := (v - v_T)^2$ into the trace identities, we obtain

$$\frac{1}{h_E}\|v - v_T\|_{L^2(E)}^2 \le \frac{1}{|T|}\|v - v_T\|_{L^2(T)}^2 + c_{10}\,\frac{2h_T}{|T|}\,\|(v - v_T)\nabla v\|_{L^1(T)},$$

where $c_{10} \in \{1/2, 1\}$ for a triangle and rectangle, respectively. The L^2-norm is estimated by the Poincaré estimate. The L^1-norm is estimated by the Cauchy and the Poincaré estimate which yields

$$\|(v - v_T)\nabla v\|_{L^1(T)} \le \|v - v_T\|_{L^2(T)}\|\nabla v\|_{L^2(T)} \le c_9 h_T \|\nabla v\|_{L^2(T)}^2.$$

Altogether, we prove the trace inequality (A.1) with the constant

$$c_8^2 = c_9 \frac{h_T^2}{|T|}(c_9 + 2c_{10}). \tag{A.4}$$

For triangles, the quotient $h_T^2/|T|$ depends only on the minimal angle in T. For rectangles, it is nothing but the quotient of the longest and the shortest edge. □

***Remark* A.2.** For a square T, Equation (A.4) becomes $c_8 = \big(2\pi^{-1}(\pi^{-1}+2)\big)^{1/2} \approx 1.21486$. With $h_E = h_T/\sqrt{2}$, (A.1) can thus be written as

$$\|v - v_T\|_{L^2(E)} \le c_{11} h_T^{1/2} \|\nabla v\|_{L^2(T)} \quad \text{for } v \in H^1(T), \tag{A.5}$$

with $c_{11} = 2^{-1/4} c_8 \approx 1.02157$. However, this estimate is by far not optimal. Nicaise [13] proves (A.5) with $c_{11} = (\pi \tanh \pi)^{-1/2} \approx 0.56524$ by some eigenvalue analysis.

References

[1] M. Ainsworth, J.T. Oden: *A posteriori error estimation in finite element analysis*, John Wiley & Sons, 2000.

[2] M. Bebendorf: *A note on the poincaré inequality for convex domains*, Z. Anal. Anwendungen, 22(04):751–756, 2003.

[3] D. Braess: *Finite elemente*, Springer, Berlin, ^{2}1997.

[4] S.C. Brenner, L.R. Scott: *The mathematical theory of finite element methods*, Springer, New-York, 1994.

[5] C. Carstensen: *Adaptive finite element method*, Lecture notes, Vienna University of Technology, 2003.

[6] P.G. Ciarlet: *The finite element method for elliptic problems*, North-Holland, Amsterdam, 1978.

[7] W.J. Coirier: *An adaptively-refined, cartesian, cell-based scheme for the euler and navier-stokes equations*, PhD thesis, The University of Michigan, 1994.

[8] Y. Coudière, J.P. Vila, P. Villedieu: *Convergence rate of a finite volume scheme for a two dimensional convection-diffusion problem*, ESAIM: M2AN, 33(3):493–516, 2000.

[9] Y. Coudiére, P. Villedieu: *Convergence rate of a finite volume scheme for the linear convection-diffusion equation on locally refined meshes*, ESAIM: M2AN, 34(6):1123–1149, 2000.

[10] C. Erath: *Adaptive Finite Volumen Methode*, Diploma thesis (in German), Vienna University of Technology, 2005.

[11] R. Eymard, T. Gallouët, Raphaèle Herbin: *Finite volume methods*, Handbook of Numerical Analysis, Volume 7. Elsevier Science B.V., first edition, 1999.

[12] V. Girault, P.A. Raviart: *Finite element methods for Navier-Stokes equations*, Springer, Berlin, 1986.

[13] S. Nicaise: *A posteriori error estimations of some cell-centered finite volume methods*, SIAM J. Numer. Anal., 43(04):1481–1503, 2005.

[14] L. E. Payne, H. F. Weinberger: *An optimal poincaré inequality for convex domains*, Arch. Rational Mech. Anal. 5, 286–292, 1960.

[15] R. Verfürth: *A review of a posteriori error estimation and adaptive mesh-refinement techniques*, Wiley-Teubner, 1996.

University of Ulm, Institute for Numerical Mathematics, Helmholtzstrasse 18, D-89069 Ulm, Germany

E-mail address: Christoph.Erath@uni-ulm.de (corresponding author)
Fon: +49 731 50-23589
Fax: +49 731 50-23548

Vienna University of Technology, Institute for Analysis and Scientific Computing, Wiedner Hauptstrasse 8-10, A-1040 Vienna, Austria

E-mail address: Dirk.Praetorius@tuwien.ac.at
Fon: +43 1 58801-10150
Fax: +43 1 58801-10196